

Lessons learned about short and long term stability and calibration of the calorimetry response at LHC for the ATLAS Tile Calorimeter

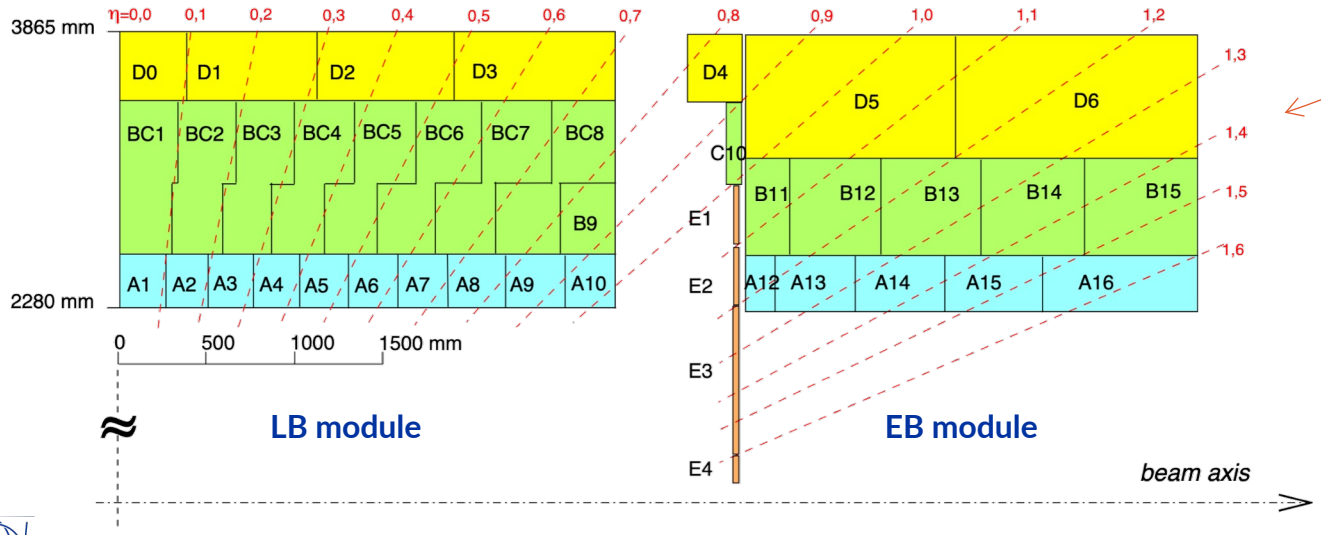
The 2026 International Workshop on the High Energy Circular Electron Positron Collider

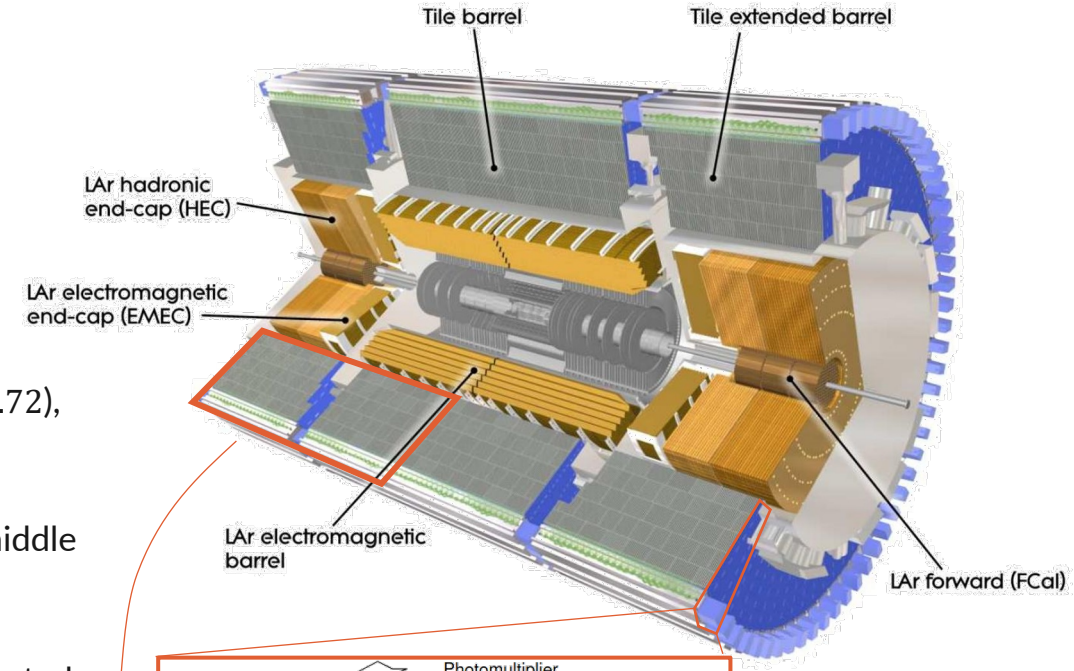
October 23, 2026

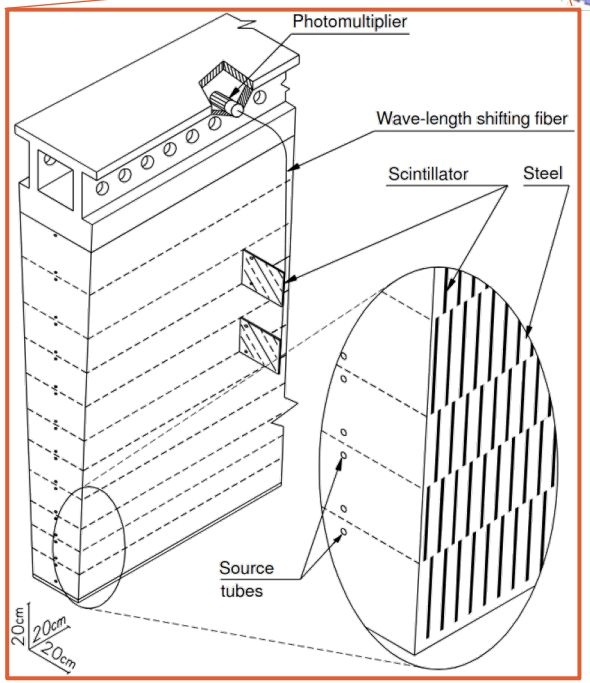
Antonio Jesús Gómez Delegido (CERN) on behalf of the ATLAS collaboration

The ATLAS Tile calorimeter

- **Tile calorimeter (TileCal): central hadronic calorimeter** of ATLAS, covering $|\eta| < 1.72$, and contributing to the reconstruction of **jets,** $\boldsymbol{E_{\mathrm{T}}^{\mathrm{miss}}}$ and $\boldsymbol{\tau}$**-leptons**.
- **Sampling calorimeter** based on **steel absorbers** and **plastic scintillator tiles**.
- **Geometry**: one **long barrel** (LB, $|\eta| < 1.0$) and two **extended barrels** (EB, $0.8 < |\eta| < 1.72$), split into four readout partitions.
- **Segmentation:** each barrel is divided into **64 modules** in azimuth ($\Delta\phi \cong 0.1$); cells are arranged in **three radial layers** with granularity of $\Delta\eta \times \Delta\phi = 0.1 \times 0.1$ in the inner and middle layer (A, B/BC) and 0.2×0.1 in the outer layer (D). Additional E cells instrument the gap/crack region between the long and extended barrels.
- **Light collection**: light collected by two wavelength-shifting (WLS) fibers per tile, connected to two **photomultiplier tubes (PMTs)**; grouping of fibers defines cell segmentation (~5000 cells).



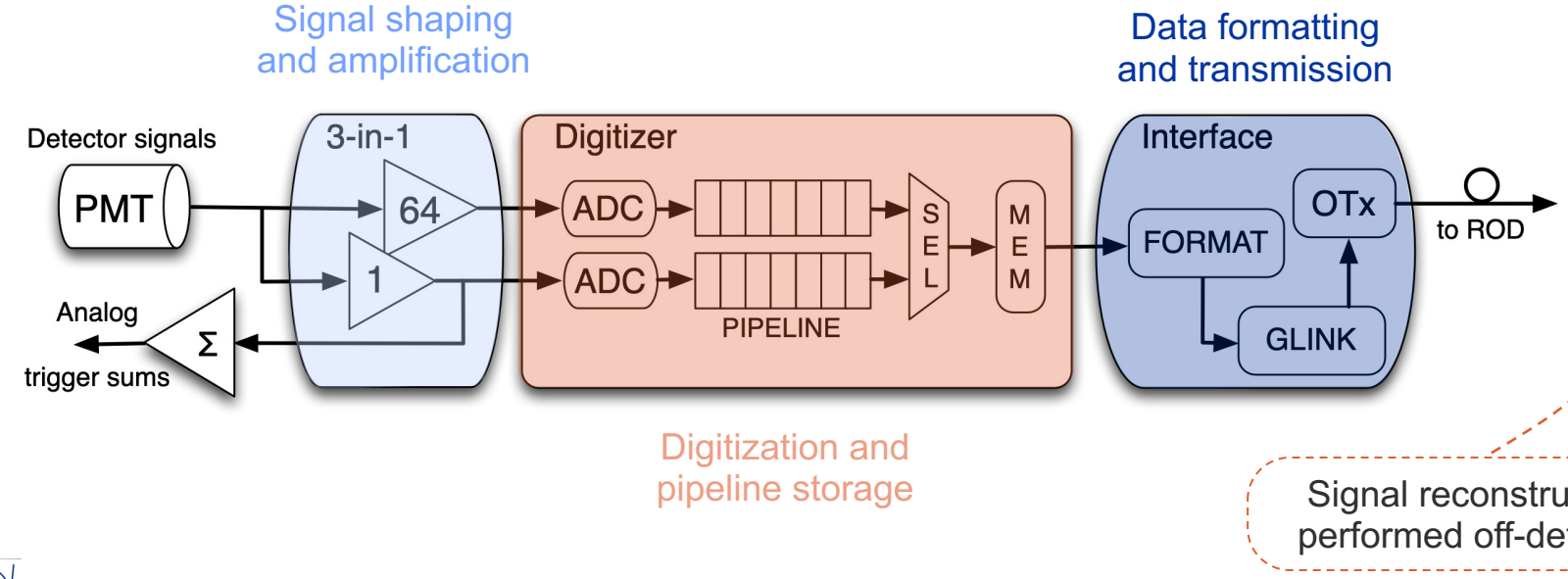




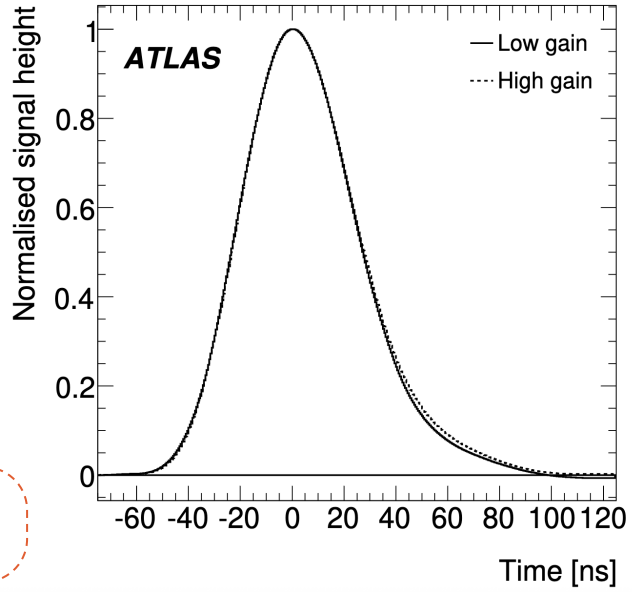
TileCal module

Tile Calorimeter readout and signal reconstruction

- Each cell is read out by **two independent photomultiplier tubes (PMTs)** (nominal gain ~10^5), providing **~10000** electronic **channels**.
- PMT pulses are amplified and shaped by front-end electronics to a characteristic width of **~50 ns FWHM**, amplitude **proportional to the collected charge**.
- Two gain branches cover a large dynamic range: **high gain** (HG, 0–12 GeV) and **low gain** (LG, 12–800 GeV) per channel (HG/LG = 64:1).
- Both gains are sampled at **40 MHz (25 ns)** using 10-bit ADCs (effective dynamic range of ~16 bits with dual gain).
- **7 consecutive samples digitized**, centered around the expected pulse maximum; low gain is saved when high gain saturates.
- **Signal reconstruction:** Pulse amplitude, time offset and pedestal reconstructed from **weighted linear combinations** of the seven samples.
  - Weights minimize the **noise-induced variance**, subject to constraints from the **reference pulse shape**



Eur.Phys.J.C 84 (2024) 12, 1313



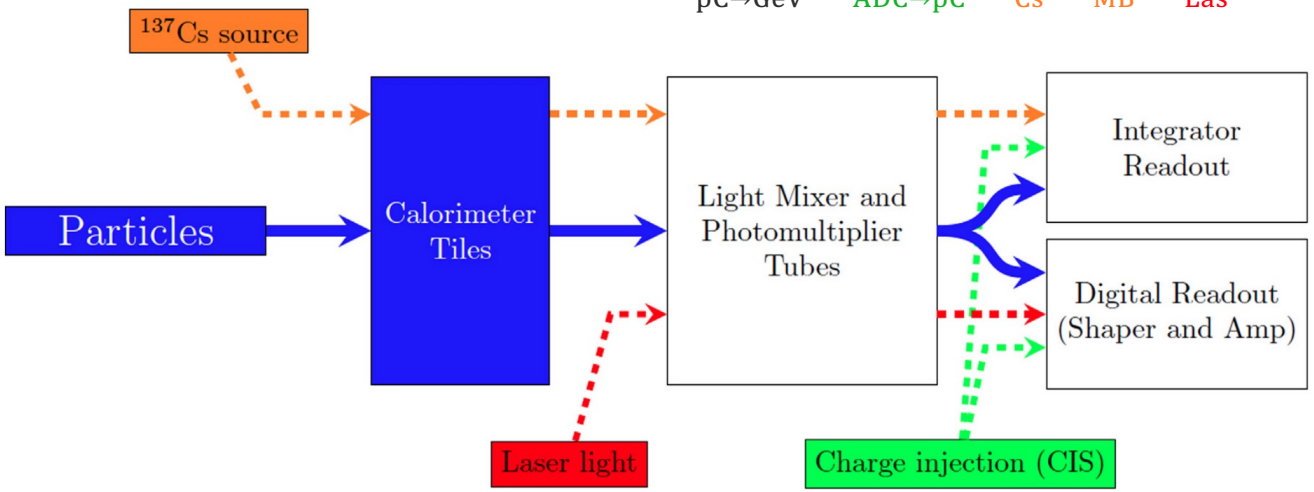
Electromagnetic scale and calibration

- **Absolute electromagnetic (EM) scale** established with ~11% of TileCal modules in test beams (2001–2003).
  - Electrons (20–180 GeV) to determine the **energy/charge conversion** in the A layer: $C_{\mathrm{pC}\to\mathrm{GeV}} = 1.05\ \mathrm{pC/GeV}$, **2.4% RMS cell-to-cell.**
  - **Muons** were used to transfer the EM scale to the **other radial layers (B/BC and D)**.
- Response to cesium-137 source used to **reproduce the test-beam reference** response through high-voltage (HV) equalization, repeated at the beginning of each LHC Run.
- **To correct for drifts in detector response,** complementary **calibration systems** monitor different parts of the readout chain and provide the corresponding corrections.

$$E[\mathrm{GeV}] = \frac{A[\mathrm{ADC}]}{C_{\mathrm{pC}\to\mathrm{GeV}} \times C_{\mathrm{ADC}\to\mathrm{pC}} \times C_{\mathrm{Cs}} \times C_{\mathrm{MB}} \times C_{\mathrm{Las}}}$$

Cs system

- Movable Cs source passing through calorimeter.
- Full optical chain: scintillator + fibers + PMTs
- Integrator readout (different from physics).
- Minimum-bias interactions provide complementary monitoring.



Charge injection system (CIS)

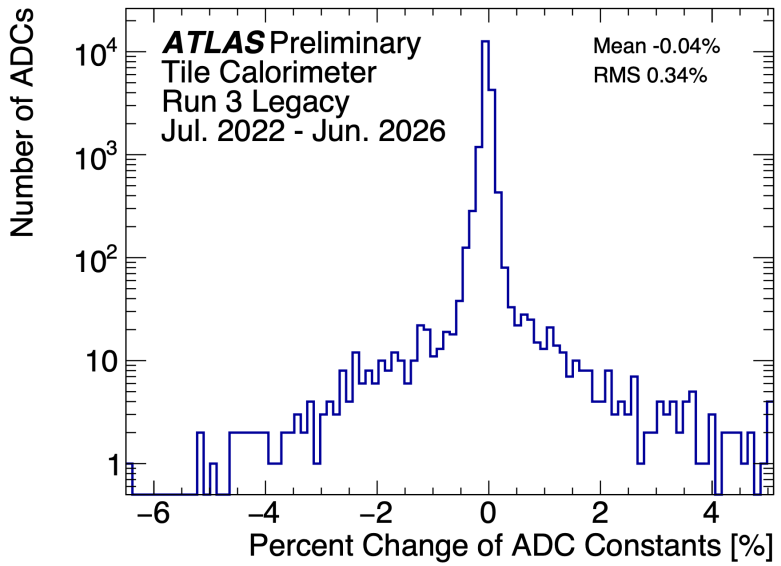
- **Electronics calibration** through injection of known charge.
- Calibrates the fast and integrator readout electronics.

Laser system

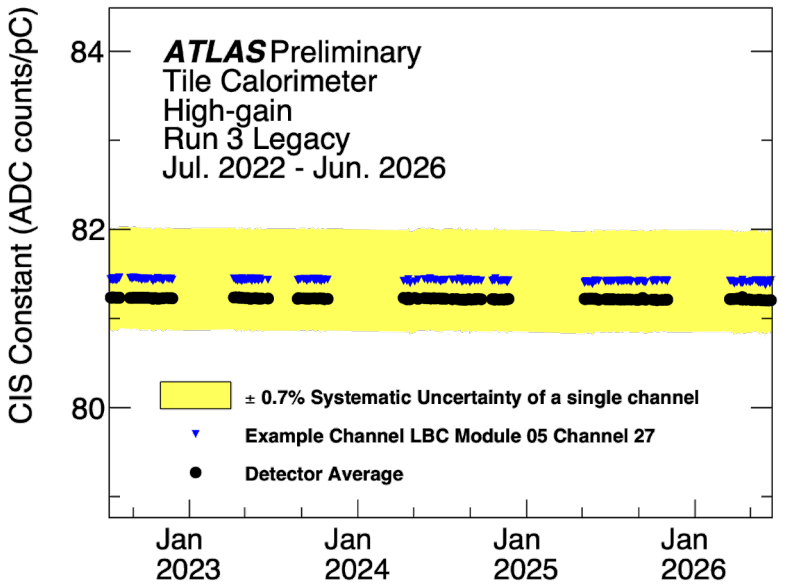
- PMTs illuminated with controlled amount of light.
- Track **PMT drift w.r.t. last Cs scan**.
- Same readout as physics.

Charge injection system

- A known charge is injected into the front-end electronics, independently of the PMTs, using precision calibration capacitors (100 pF).
- Dedicated charge scans cover the dynamic range of both gains, measuring the reconstructed amplitude as a function of injected charge.
  - Linear fits determine the **ADC-to-pC conversion factors** for each channel and gain. Calibration runs are performed twice a week, with constants updated monthly or more frequently if needed. **Precision ~0.7%**
- Excellent stability throughout Run 3 (2022–2026), with **no significant systematic drift**:
  - Mean relative change of −0.02%, RMS of 0.34% across individual ADC calibration constants.
  - Detector-average run-to-run RMS/mean at the per-mil level (0.011% in HG and 0.008% in LG).
- However, the stability does **not imply a perfectly linear response** in the full dynamic range.



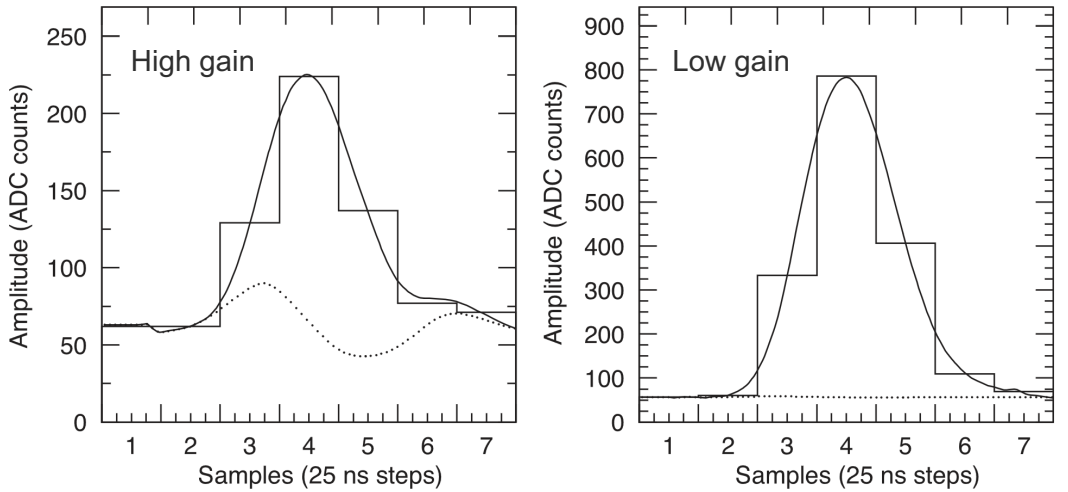
Charge injection system (CIS) public plots



Charge injection system: critical points

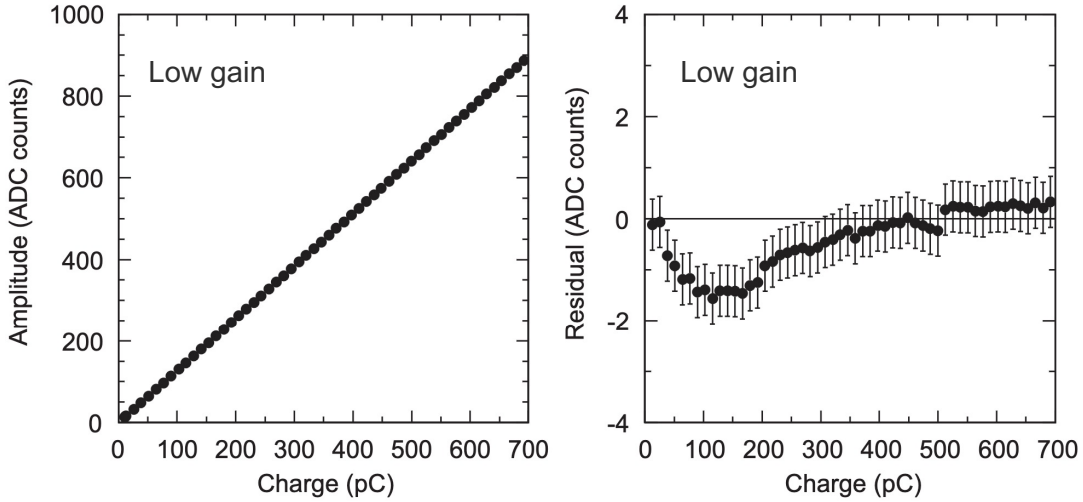
- Accurate CIS calibration requires understanding effects **beyond** a **linear charge-to-ADC conversion**. Two characteristic examples:
  - **Leakage pulse**: CIS injection circuitry introduces a spurious bipolar pulse through parasitic capacitances.
    - Present only in CIS signals; relatively important at **small injected charges**.
    - Measured with zero-charge injections and accounted for in the reconstructed pulse amplitude.
    - **HL-LHC electronics reworked to minimize effect.**
  - **Low-gain nonlinearity**: Saturation of the HG amplifier affects the low-gain response through their shared input.
    - Charge-dependent deviation of up to **~2% around 100 pC**.
    - Characterized and corrected using a **global nonlinear calibration correction**.
- **Lesson learned**: good electronics understanding and characterization of these small effects is crucial to control residual non-linearities.

Leakage pulses in CIS events (HG and LG)



Nucl.Instrum.Meth.A 606 (2009) 362-394

Non-linearity in residuals

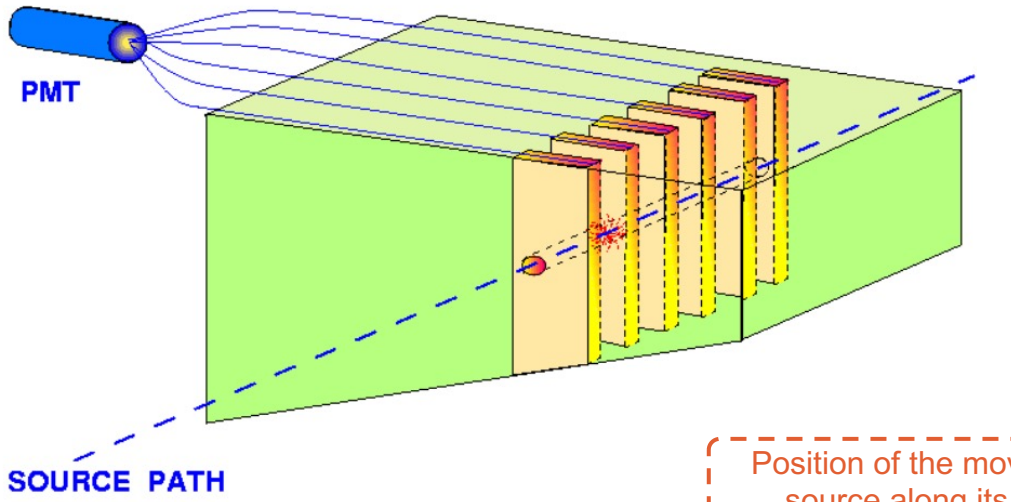


Cesium system

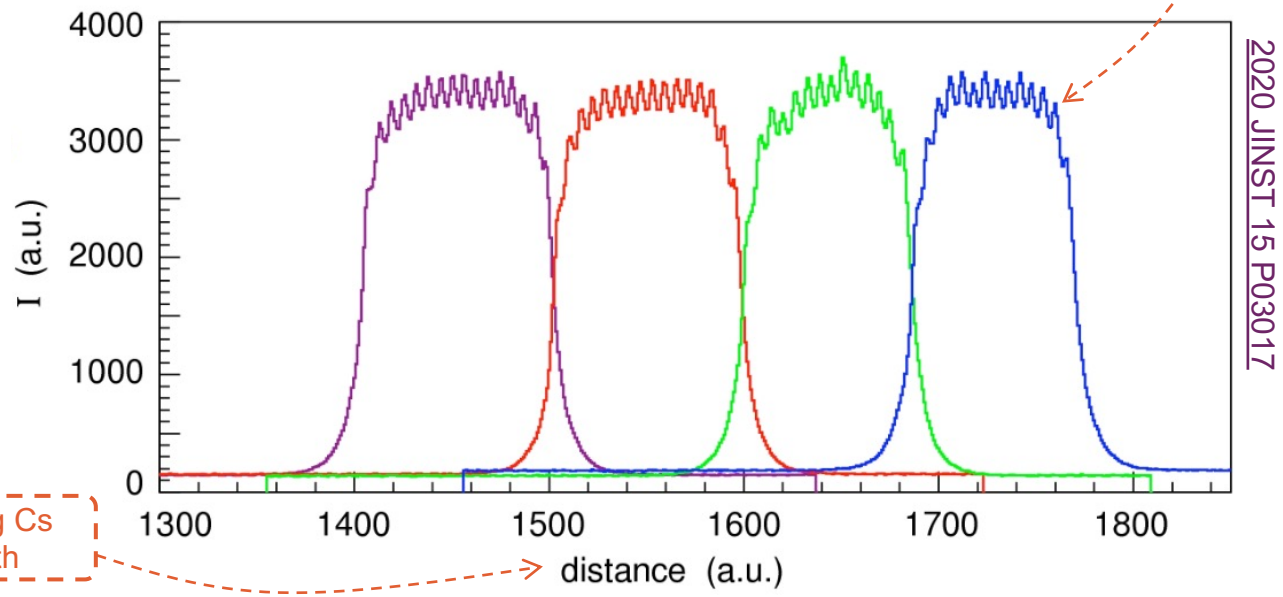
- **Movable Cs source (662 keV γ-rays) is hydraulically driven through tubes crossing the scintillator tiles.**
  - The induced scintillation light is measured using the **slow integrator readout (**10–20 ms integration time), with monthly calibration scans.
- Sensitive to variations in the response of **scintillators, WLS fibers and PMTs.**
- Individual tile responses can be resolved, allowing the identification of optical defects. Precision of the system ~0.2–0.3%.
- **Cs measurements provide a common reference to equalize the calorimeter response through PMT HV adjustments.** Subsequent scans track response drifts and provide corrections to preserve the energy calibration.

Small peaks: Individual scintillator tile responses.

Cs calibration concept



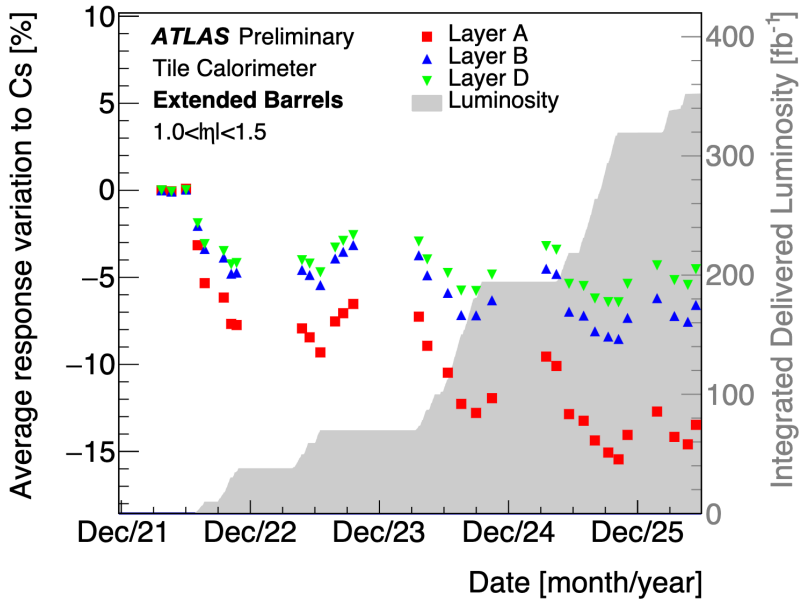
PMT response in four neighboring cells (in different colors)

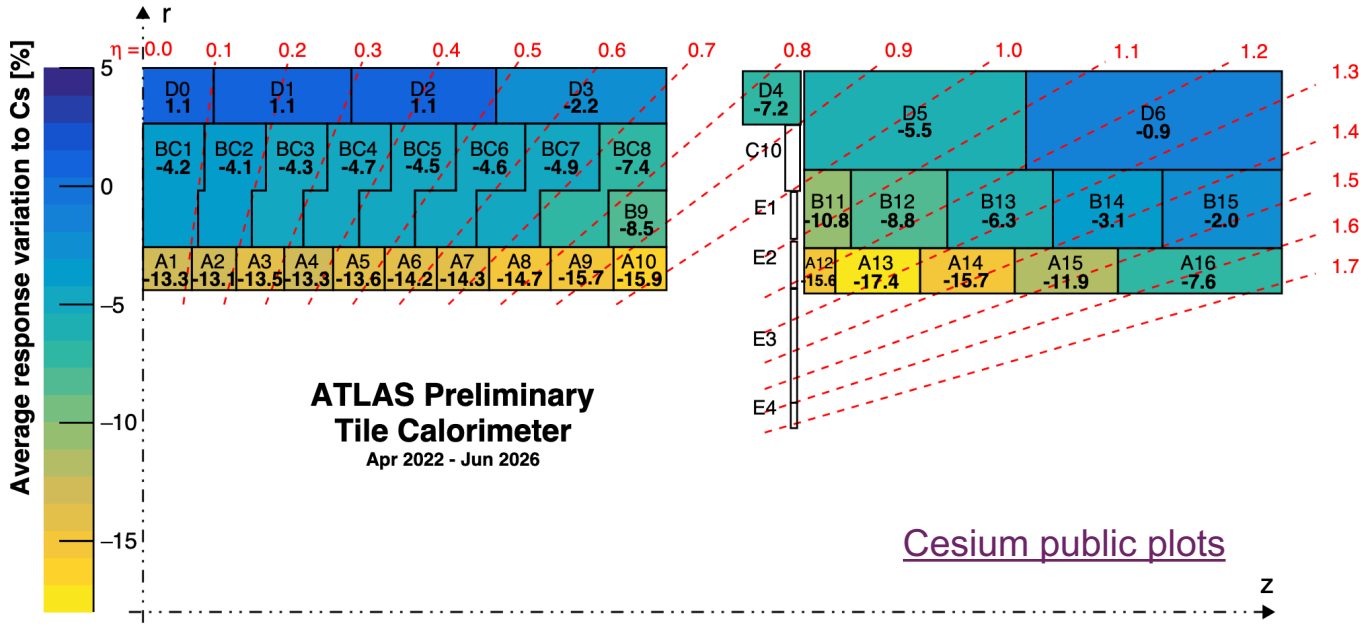


Position of the moving Cs source along its path

Cesium system

- **Movable Cs source (662 keV γ-rays) is hydraulically driven through tubes crossing the scintillator tiles.**
  - The induced scintillation light is measured using the **slow integrator readout** (10–20 ms integration time), with monthly calibration scans.
- Sensitive to variations in the response of **scintillators, WLS fibers and PMTs.**
- Individual tile responses can be resolved, allowing the identification of optical defects. Precision of the system ~0.2–0.3%.
- **Cs measurements provide a common reference to equalize the calorimeter response through PMT HV adjustments.** Subsequent scans track response drifts and provide corrections to preserve the energy calibration.
- **Long-term response evolution:** stronger response degradation in the inner A layer, increasing with accumulated luminosity, with partial recovery during periods without collisions.



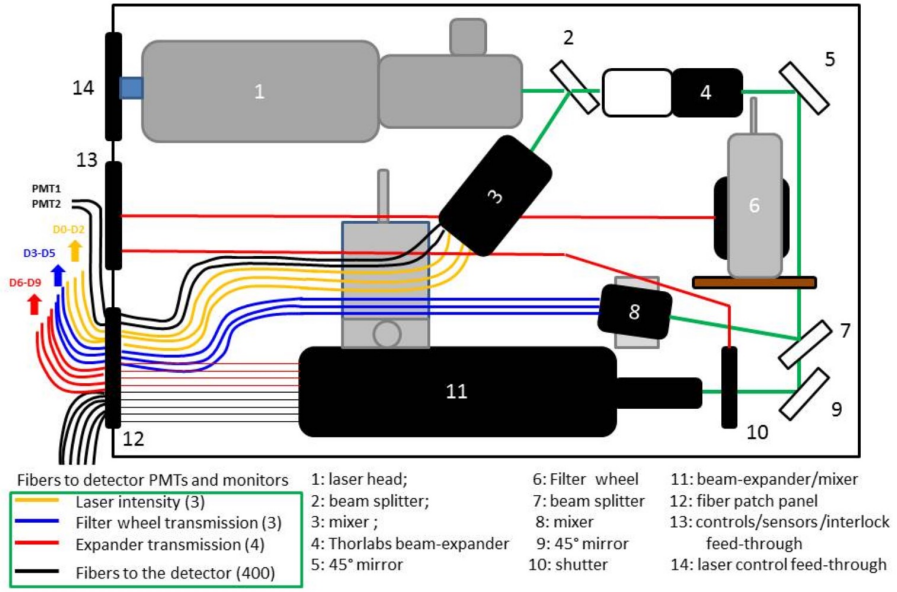


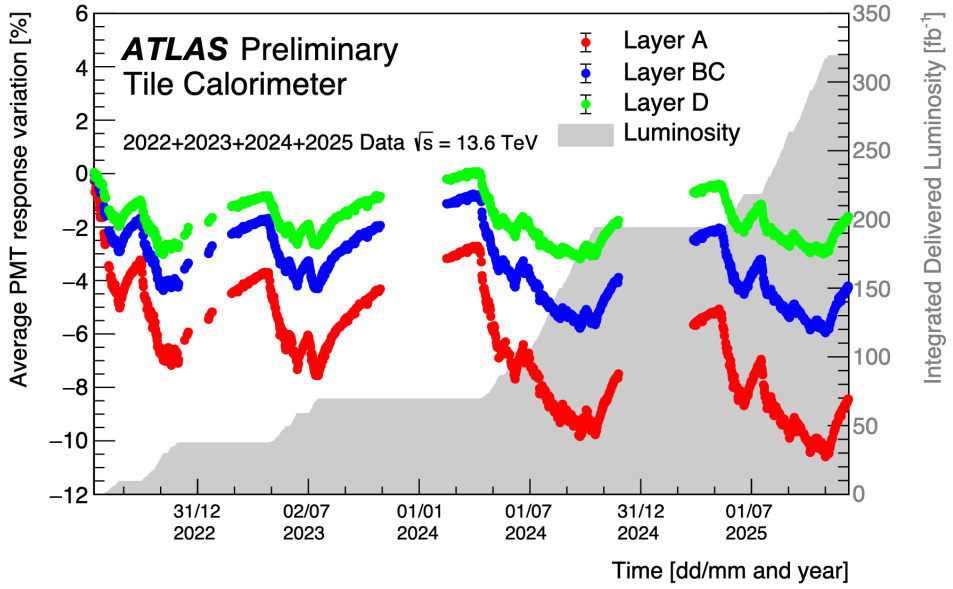
Cesium public plots

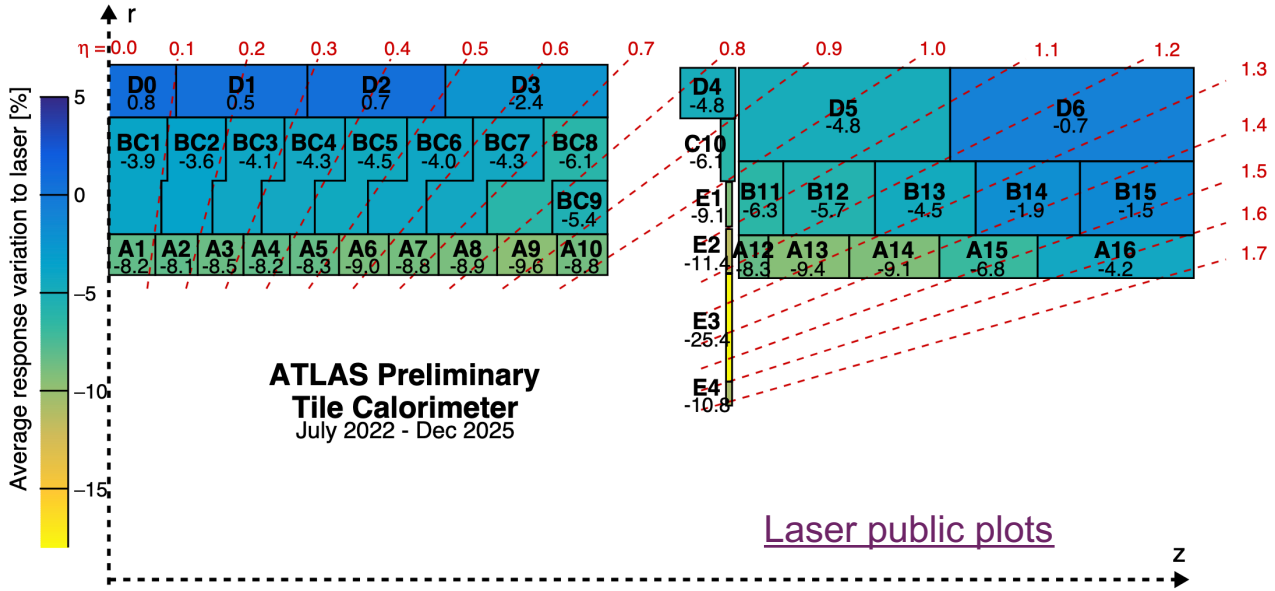
Laser system

- **Short light pulses** (532 nm) are **distributed** to the **PMTs** through a network of ~400 long clear fibers (bypassing scintillators and WLS fibers).
- **Pulse amplitude** is normalized to the monitored laser intensity (diodes in optics box) and **compared with a reference around** the latest **Cs calibration**.
- Daily calibration, **fast drifts in PMTs** between Cs scans. **Precision ~0.5%.**
- **Significant long-term** response **evolution** with luminosity-dependent PMT response variations.
  - **Strongest response losses** in the **inner** A **layer**, followed by BC and D; partial **recovery** observed during periods **without collisions**.

2023 JINST 18 P06023



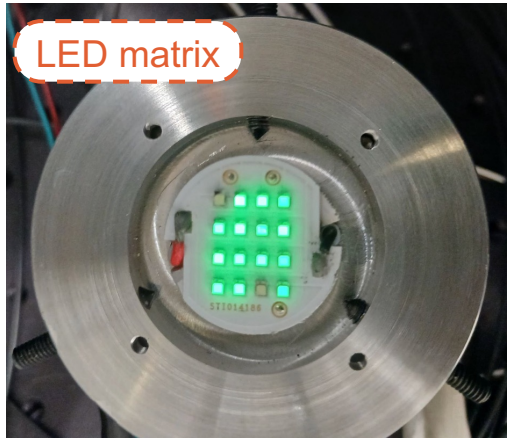


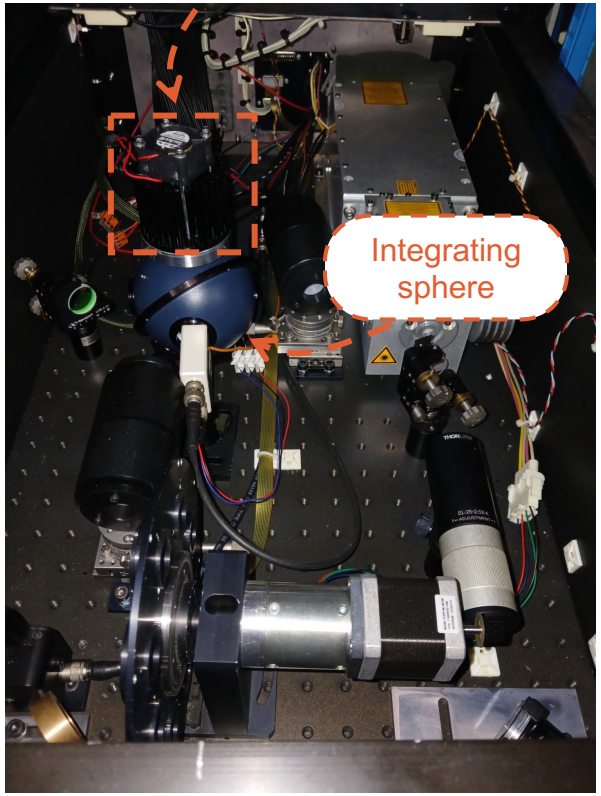


Laser public plots

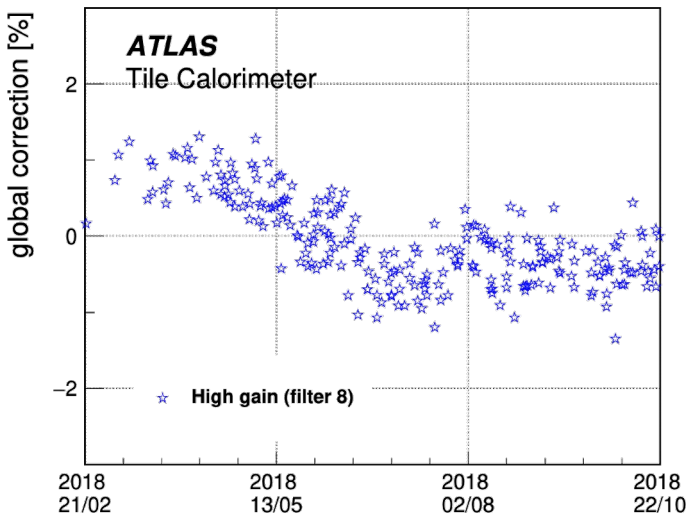
Laser system: critical points

- Laser calibration must correct for PMT response drifts, not changes in light delivered to the PMTs or instabilities in optics box.
  - **Variations** in **light distribution, fiber transmission and reference photodiodes** are **monitored precisely** and corrected.
  - After correcting for them, **laser and Cs measurements agree within 0.4%.**
- **Dependence on anode current**: average **current induced by collisions** can **modify the voltage distribution** across the PMT dynodes, affecting the response.
  - **Up to ~2–3% observed in highly exposed cells.**
  - For **HL-LHC:** active dividers will mitigate the effect, and an integrating sphere will combine laser pulses with **continuous LED illumination** to **reproduce collision-like anode currents**.

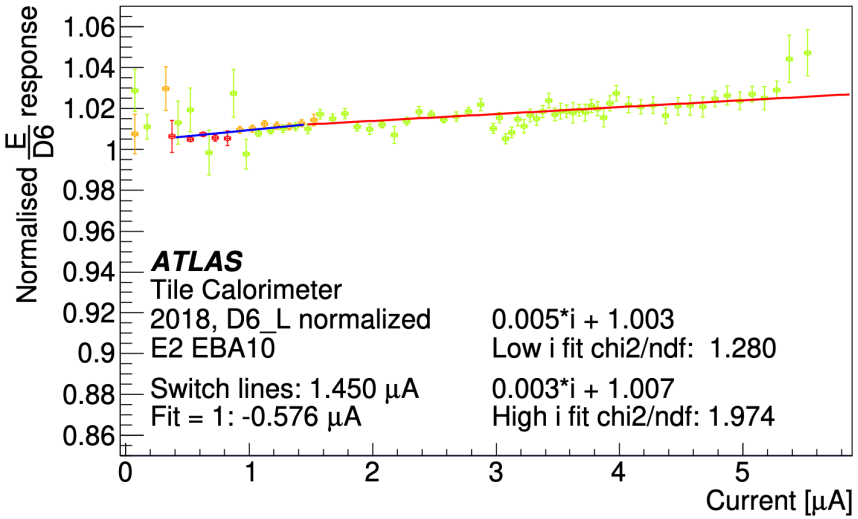




2023 JINST 18 P06023

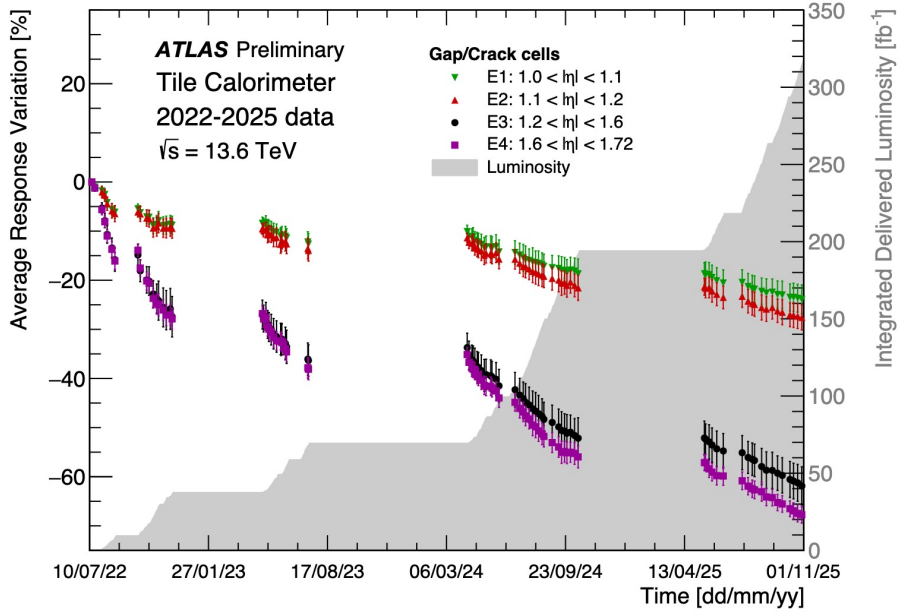


2023 JINST 18 P06023

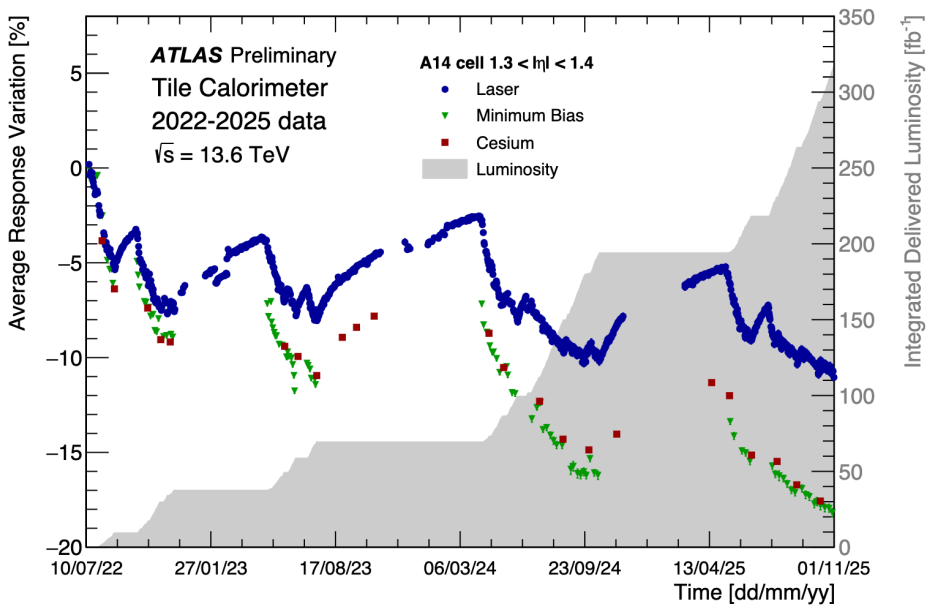


Calibration using minimum bias interactions

- Minimum-bias (MB) interactions produce PMT currents approximately proportional to the instantaneous luminosity. Slow readout used to record them independently of the fast physics readout. Monitors variations in the full optical-chain response (as Cs system).
- PMT current is normalized to the independently measured track-counting luminosity and compared with a reference run.
  - MB provides calibration for detector regions where calibration with Cs source is unavailable (e.g. E cells, located between LB and EB).
  - **Strong response degradation** observed in the most exposed E cells, reaching ~68% in E4 by the end of 2025.
- MB and Cs measurements show consistent response variations (~18% decrease by the end of 2025 in A14, highly exposed), while laser measures a smaller PMT response variation. Difference interpreted as degradation in scintillator and WLS fiber.



Minimum bias public plots

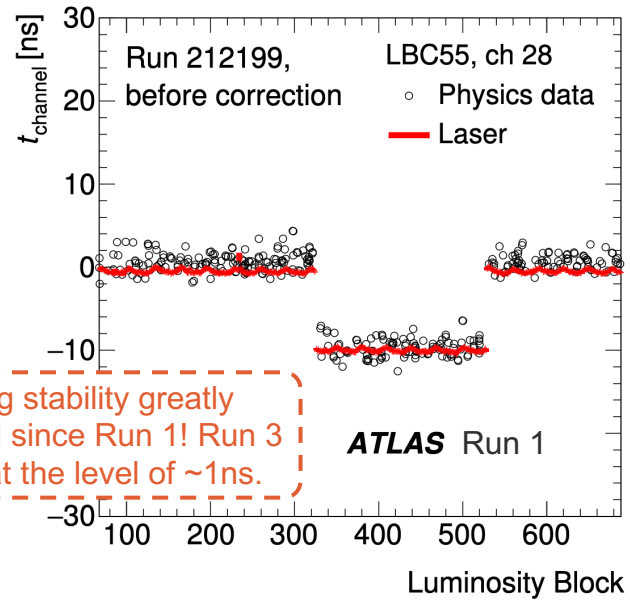


Timing calibration and performance

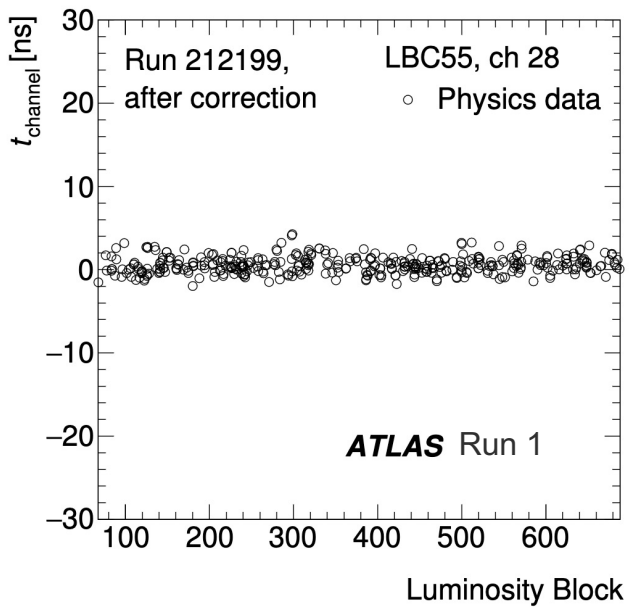
- Per-channel timing offsets are determined using collision data, aligning the reconstructed signals with the LHC bunch-crossing clock.
- Timing **monitoring**: laser pulses injected during **empty bunch crossings (without collisions)** allow continuous monitoring during physics runs.
  - Sudden **timing jumps** can be detected and **corrected offline**, restoring **timing stability below the ~1 ns level**. Important for time-of-flight measurements in ATLAS and for signal reconstruction.
- Timing performance is measured using **cells associated with jets**. Mean of the cell-time distribution probes residual misalignment, the **Gaussian width** determines the resolution.
  - At **low energies**, **pile-up** affects the resolution; additional **layer dependence** from **detector geometry**, significant at higher energies.

Timing jump corrections using laser signals

Eur.Phys.J.C 78 (2018) 12, 987

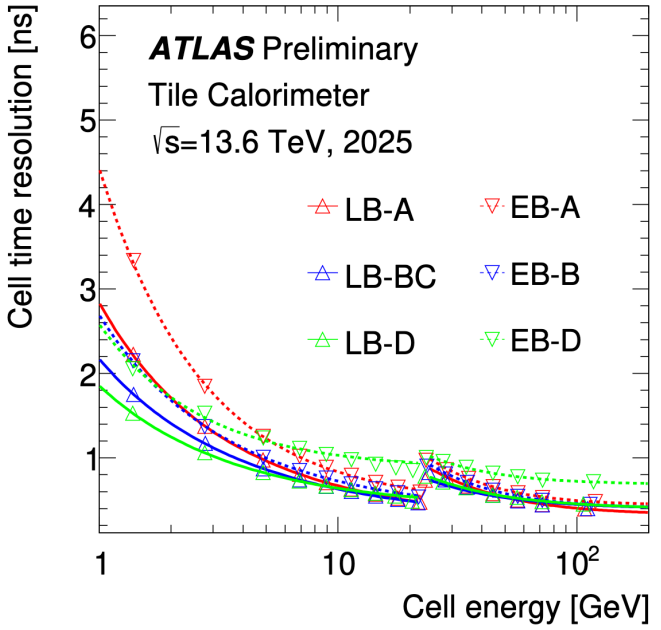


Timing stability greatly improved since Run 1! Run 3 jumps at the level of ~1ns.



Cell time resolution in 2025

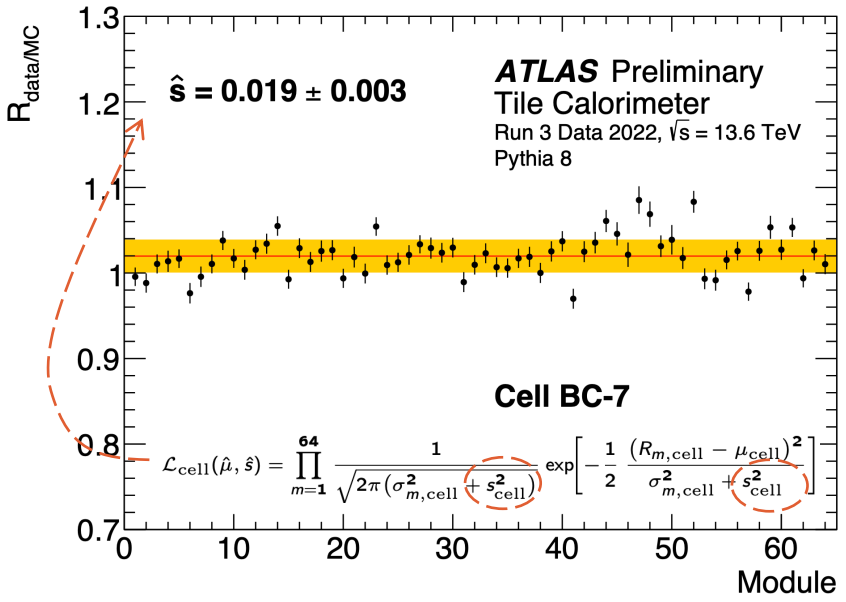
Timing public plots



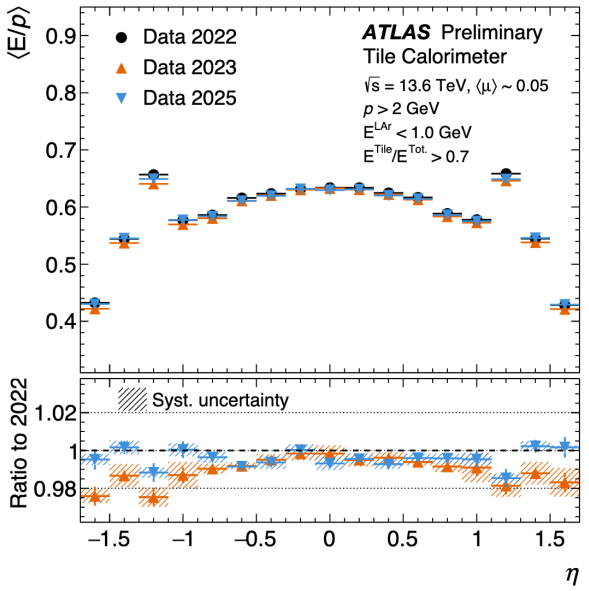
Cross-checks with collisions

- **Independent physics measurements are essential to verify that calibration preserves the actual calorimeter response.**
- Fundamental for validation of calibrated energy scale, response uniformity and long-term stability. **Two examples:**
  - **Collision muons** from W → μν decays probe the calorimeter response under normal collision conditions.
    - Truncated mean of **dE/dx (deposited energy per path length)** compared between data and simulation, testing EM scale and uniformity. **Preliminary results show ~2% azimuthal nonuniformity** measured in Run 3.
  - **Isolated charged hadrons** in low pile-up conditions probe the hadronic response through **E/p**, comparing calorimeter energy with the momentum measured by the tracking detector.
    - Measurements from **2022, 2023 and 2025** show consistent response versus η, ϕ and p; **year-to-year differences at the ~2%** level.

Non-uniformity with collision muons



Stability of E/p with isolated hadrons

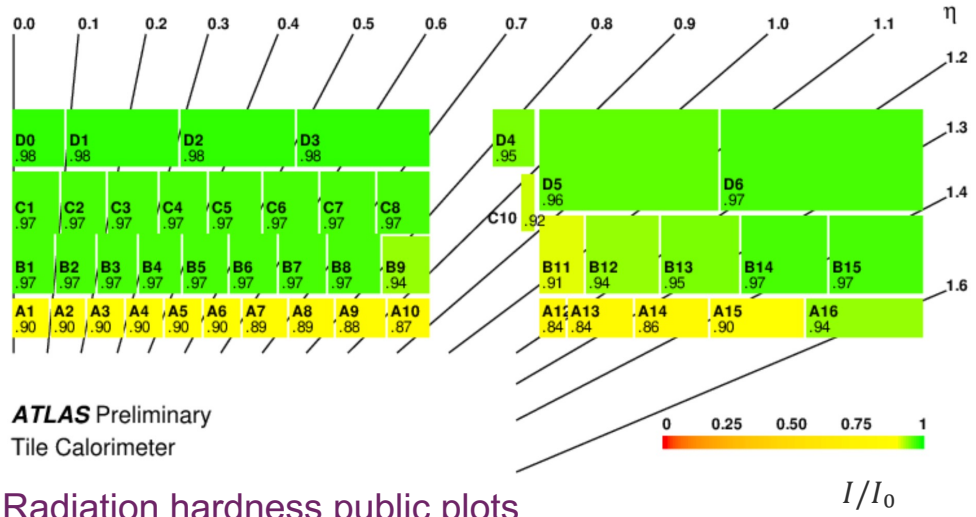


Single particle response public plots

Long-term aging: optical response degradation

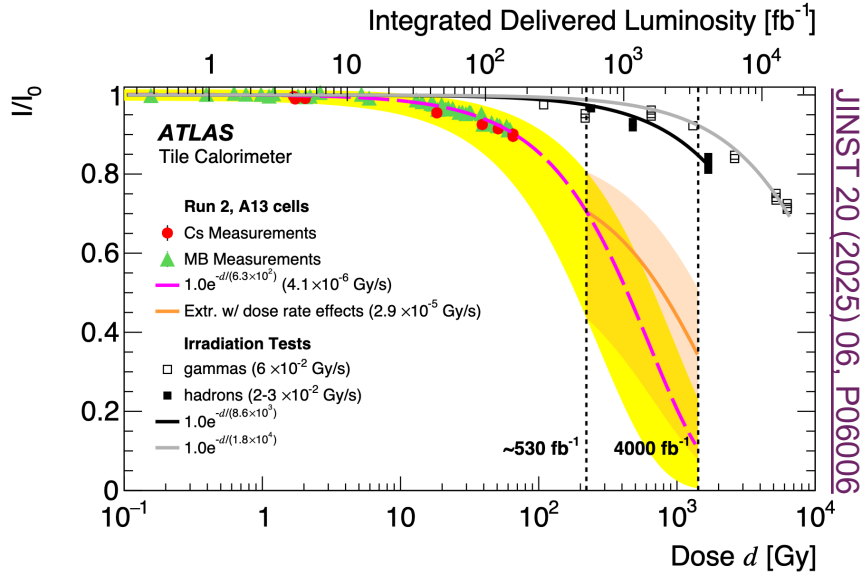
- **Radiation damage** reduces the light output of scintillators and WLS fibres. Combining Cs/MB and laser measurements isolates optical ageing from PMT response variations:
  - $I/I_0 = R_{\mathrm{Cs}}/R_{\mathrm{Laser}}$, where I/I₀ is the light yield relative to the beginning of Run 2 (2015) and R_{i} denotes the calibration response normalized to its corresponding reference measurement
- Light-yield losses reached **~15% in the most exposed A-layer cells** by the end of 2024, with much smaller degradation in other regions.
- **Radiation damage depends on both accumulated dose and dose rate**. Higher dose rates result in less degradation for the same accumulated dose. **HL-LHC extrapolations predict ~50–60% losses in typical A-layer cells after 4000 fb^{-1}** (including dose-rate effects).
- **PMT HV adjustments and calibration** corrections can **restore average response**, although the original light yield cannot be recovered.

Light yield degradation from February 2015 to November 2024



Radiation hardness public plots

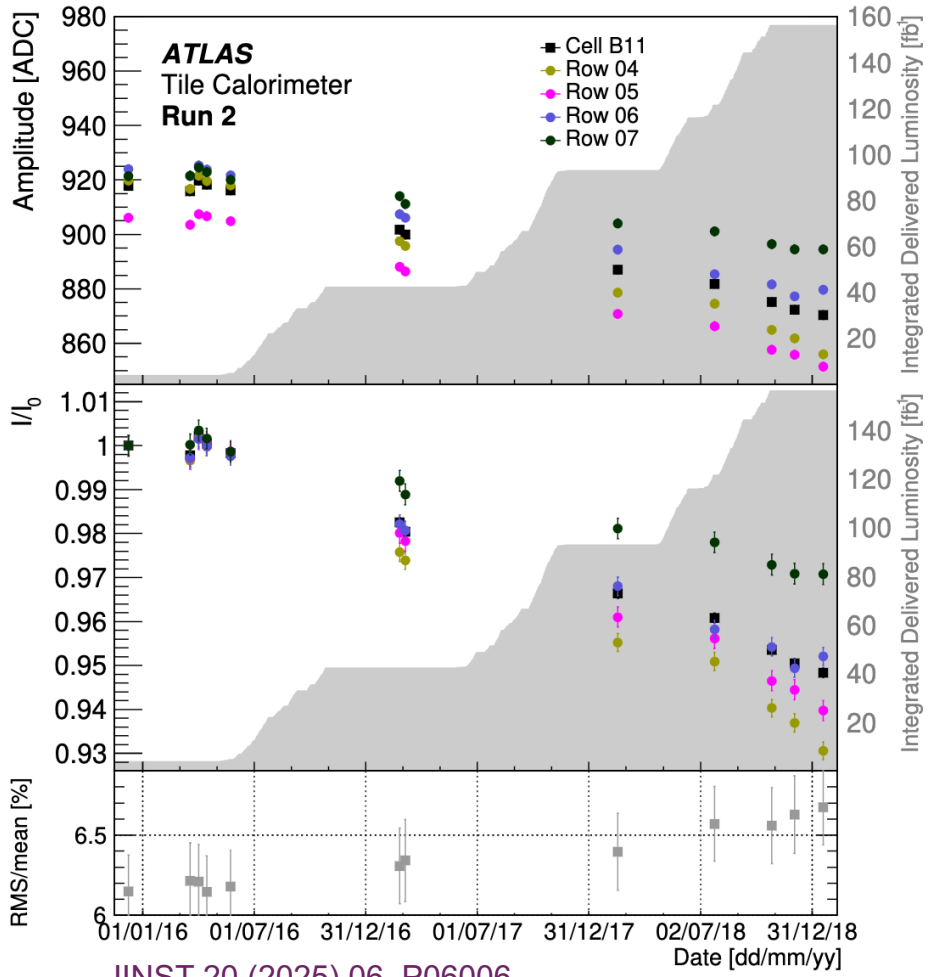
HL-LHC projections of light yield degradation in exposed cells



Long-term aging: impact on response uniformity

- **Different tiles within the same cell receive different radiation doses,** leading to different aging rates and potentially affecting response uniformity.
- **Individual tile responses can be resolved using Cs scans**, allowing the response uniformity (tile RMS/mean) to be monitored.
  - Example on the right, showing tile rows from B11 cell.
  - B11: light-yield losses ranged from ~3% to 6% across tile rows, increasing nonuniformity to ~7%.
- The measured non-uniformity did not increase dramatically during Run 2 and remained **below the 10% TileCal specification** (intended to limit impact on jet energy resolution).
- **Limitation of calibration:** cell-level corrections restore the average response but cannot remove spatial non-uniformities caused by differential ageing.

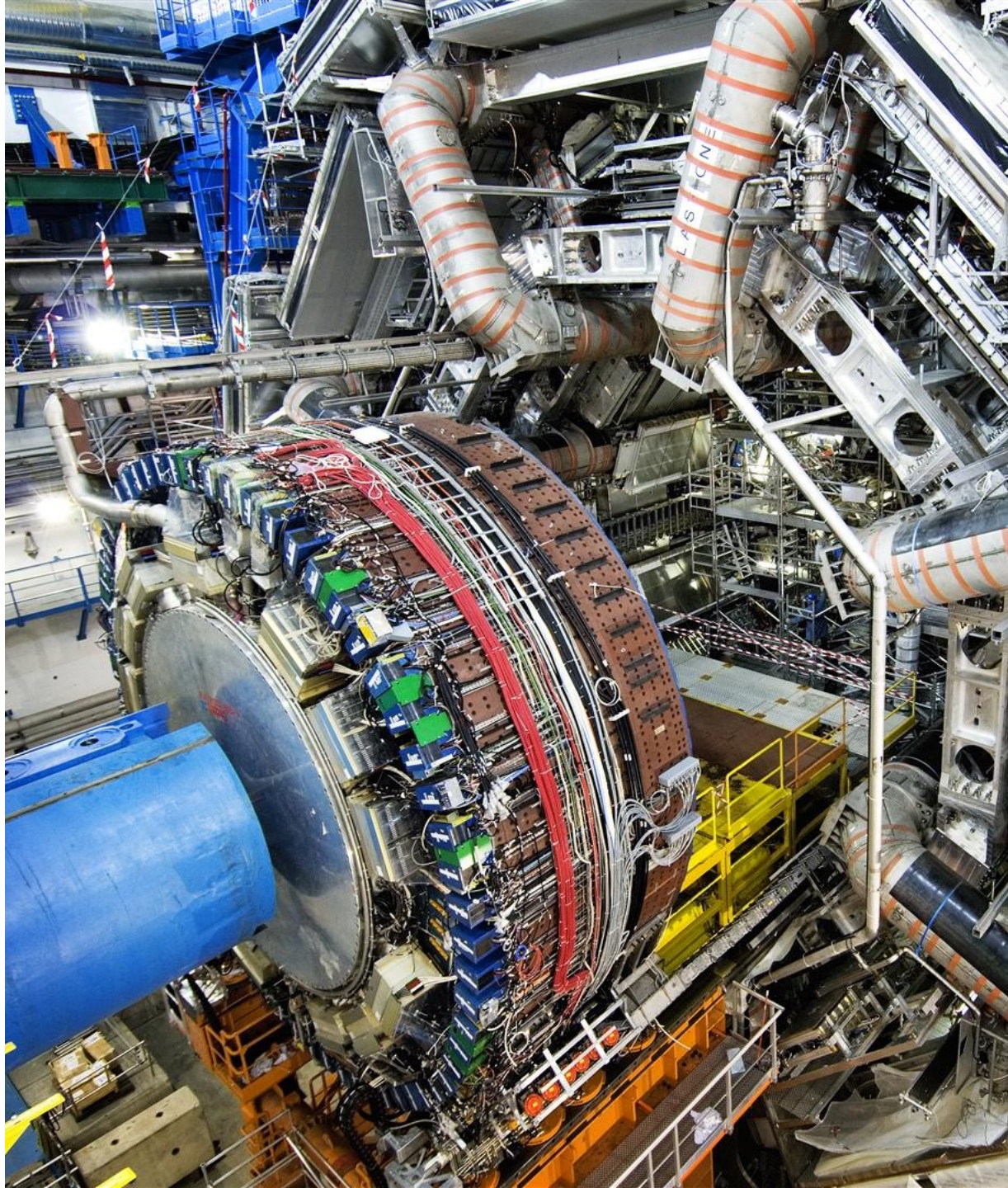
Tile row non-uniformity in B11 during Run 2



JINST 20 (2025) 06, P06006

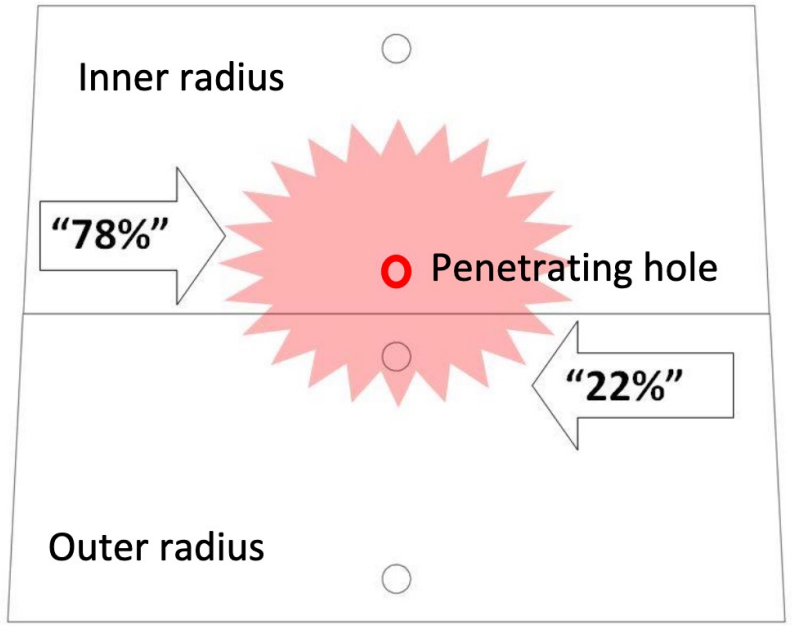
Conclusions

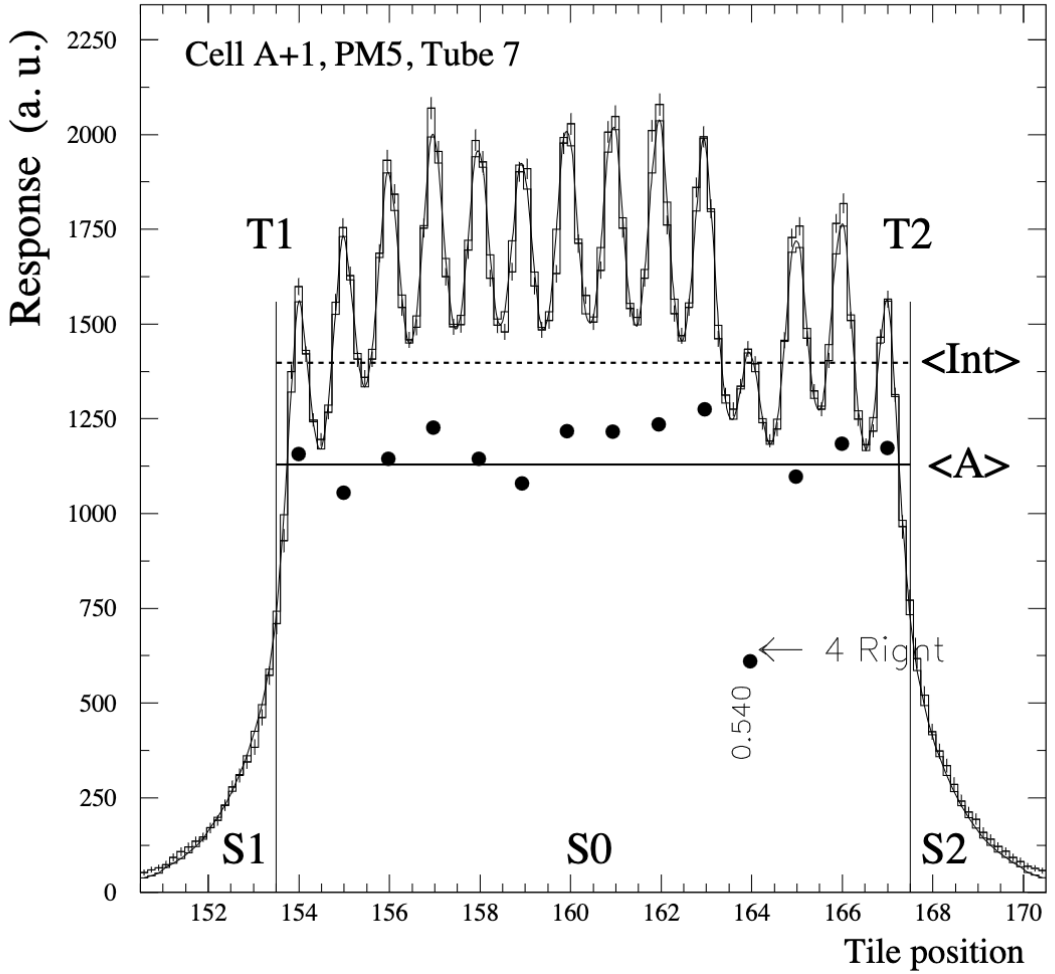
- **Tile Calorimeter's complementary calibration syst**ems monitor and correct different components of the detector response, **maintaining** the calibrated **energy response stable** at the **percent level**.
- **Precise calibration requires** a **detailed understanding** of the detector and calibration systems. Characterization of subtle effects and continuous monitoring are essential to achieve this precision.
- **Independent physics probes** are **essential** to validate the energy scale, response uniformity and long-term stability of the calibrated detector.
- **Towards HL-LHC**: HV adjustments and calibration corrections can compensate average response losses, but reduced light yield and spatial nonuniformities remain important challenges.



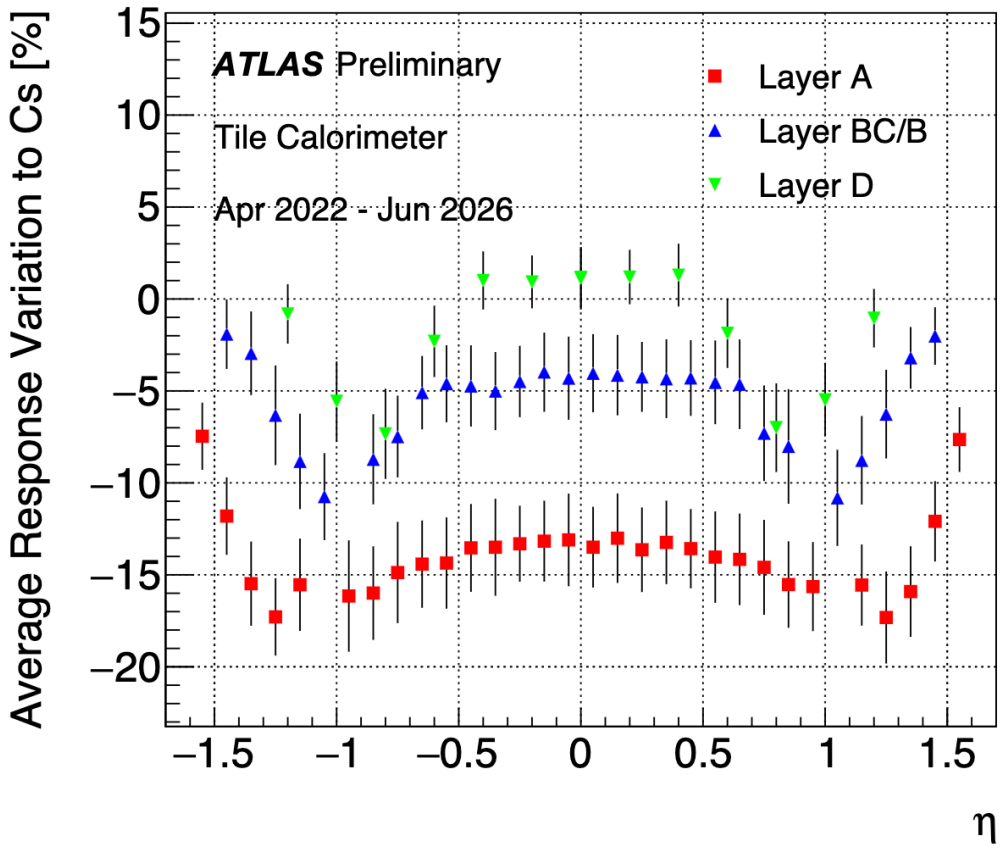
Additional slides

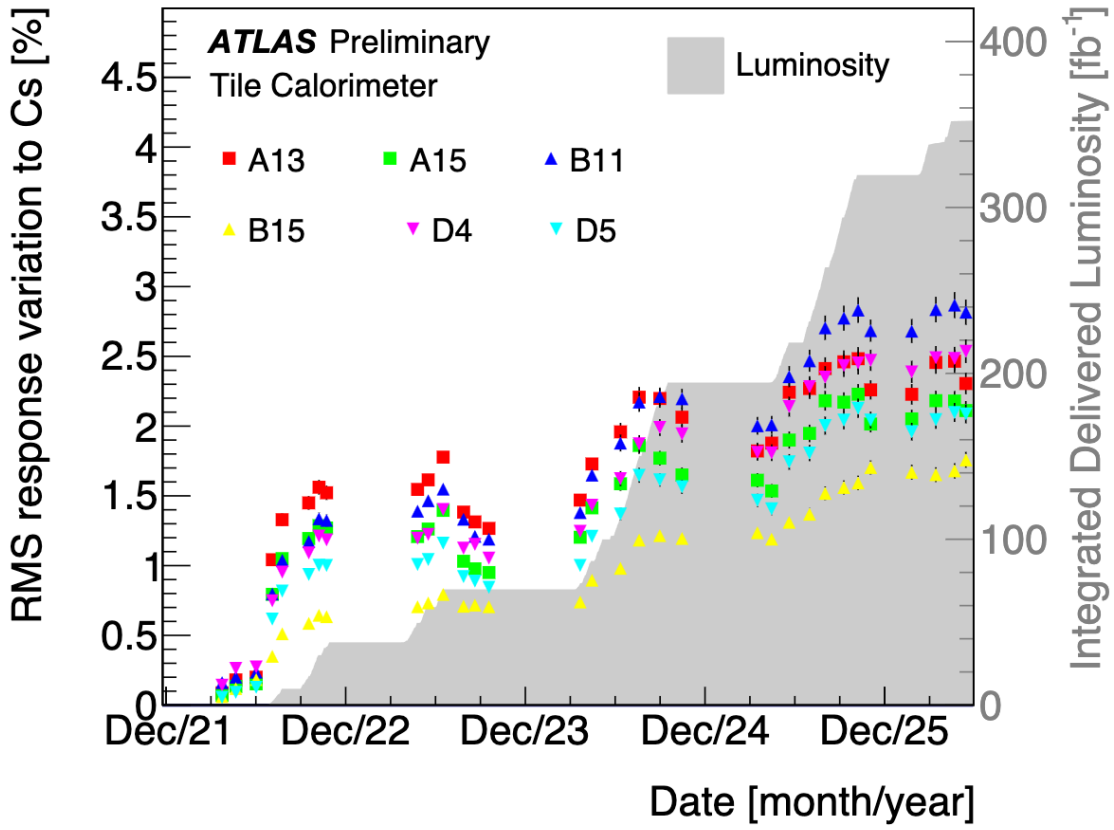
Cs method


Inner radius
"78%"
Penetrating hole
"22%"
Outer radius

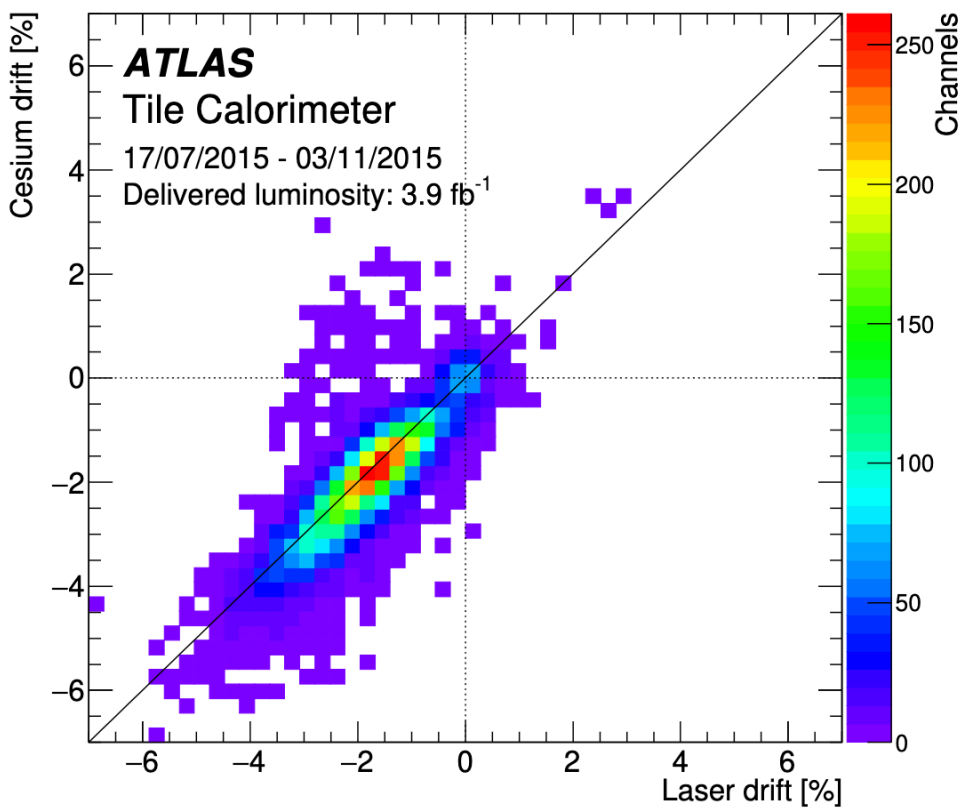

Cell A+1, PM5, Tube 7
Response (a. u.)
Tile position
T1
T2
<Int>
<A>
S1
S0
S2
4 Right
0.540
2250
2000
1750
1500
1250
1000
750
500
250
0
152
154
156
158
160
162
164
166
168
170

Cs calibration

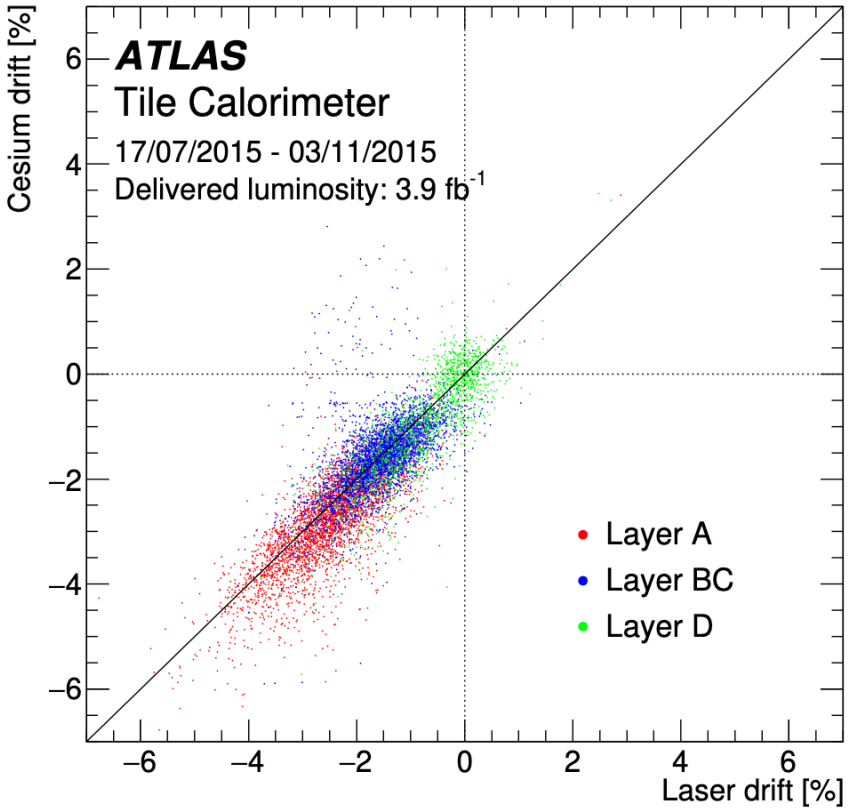




Laser validation

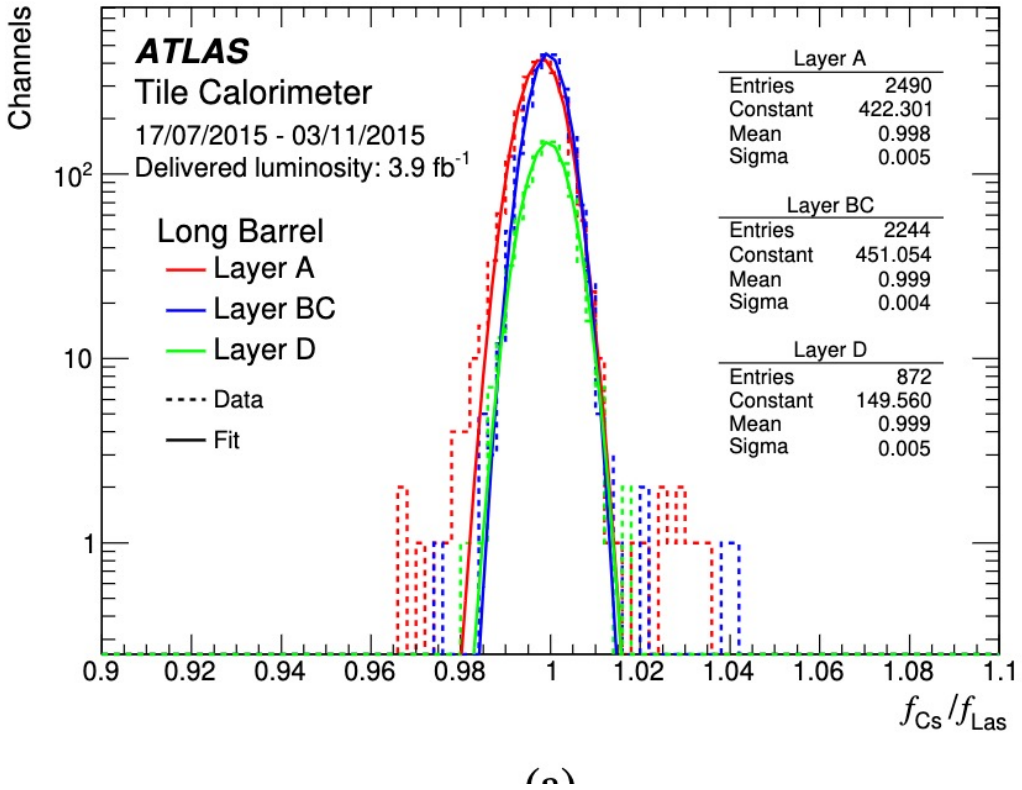


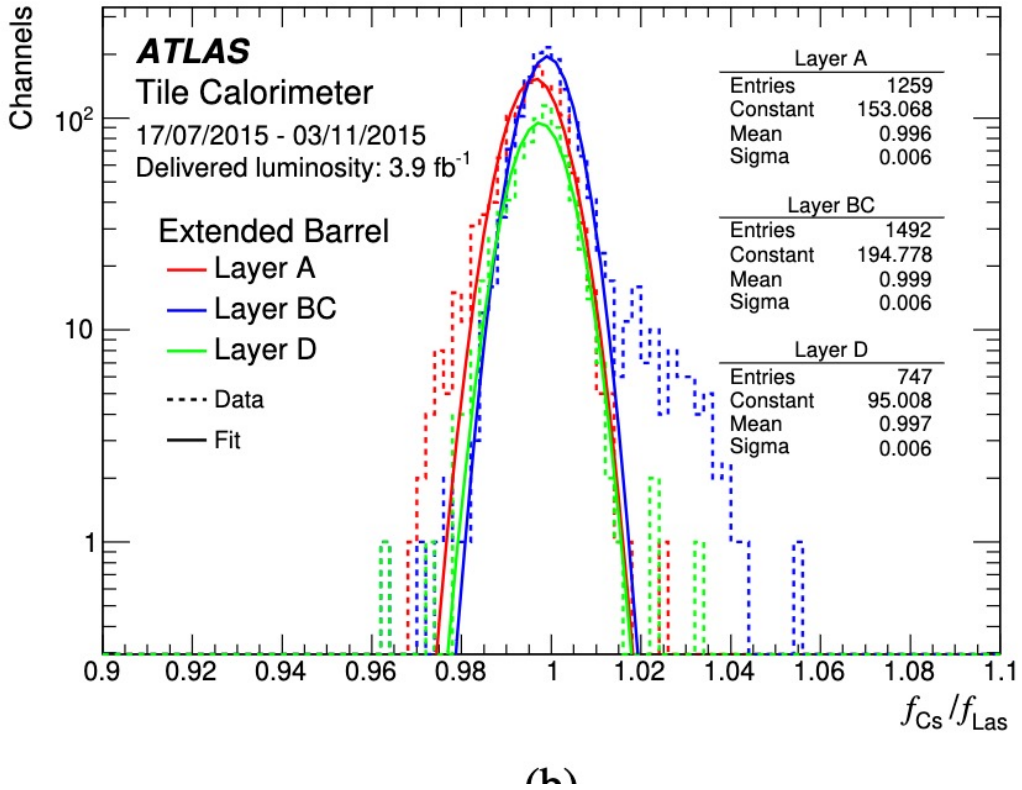
(a)



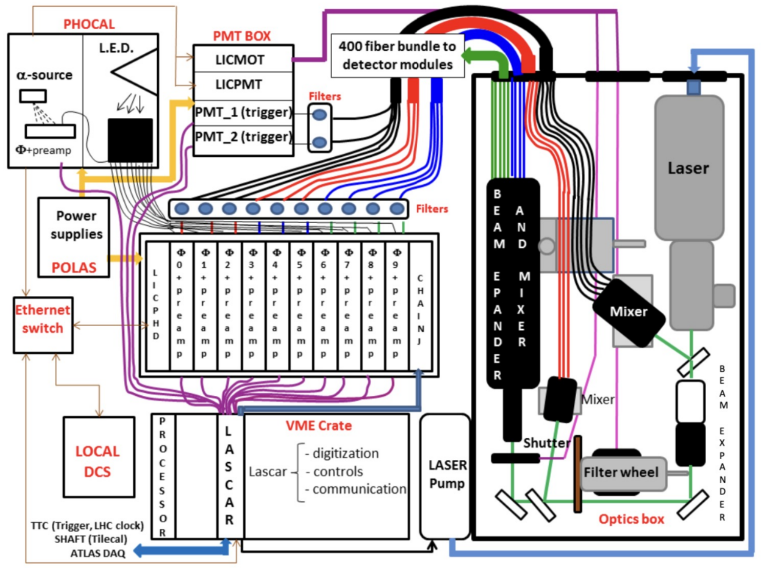
(b)

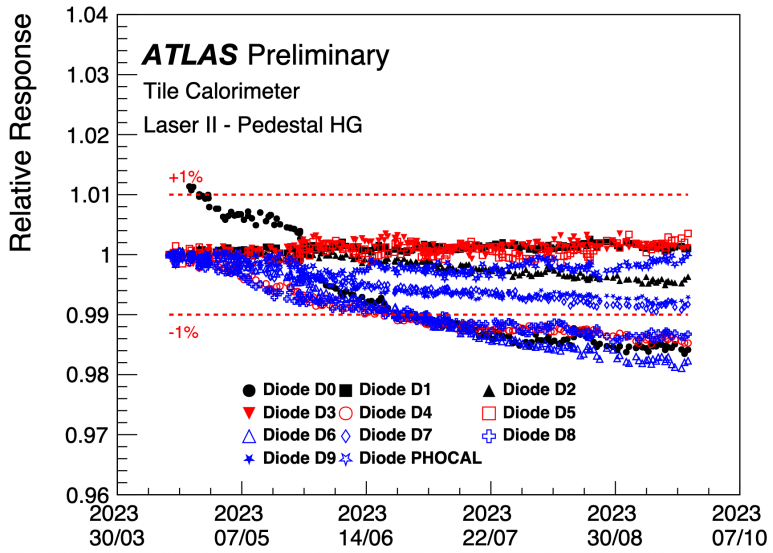
Laser validation

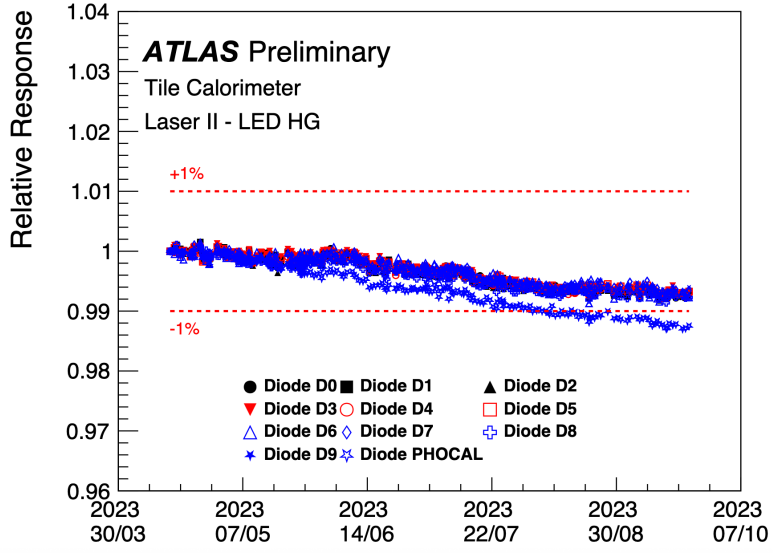


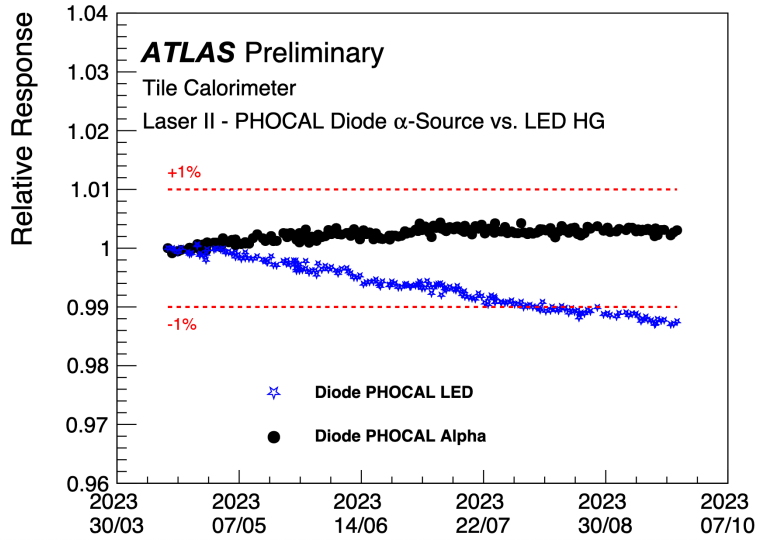


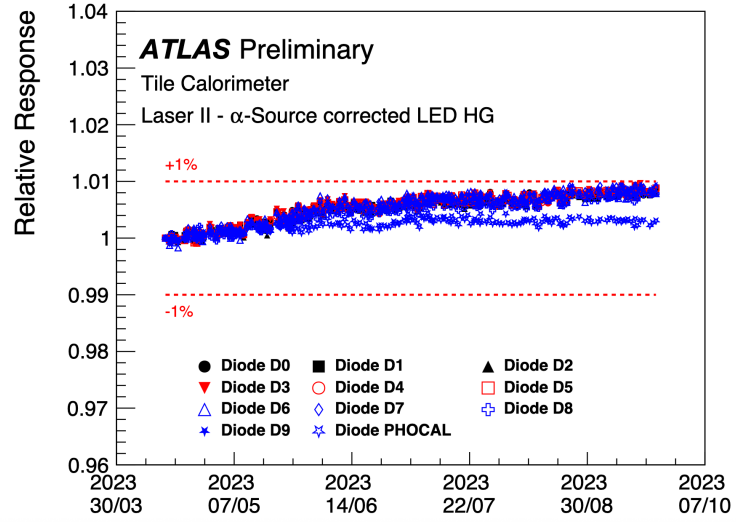
Laser system stability



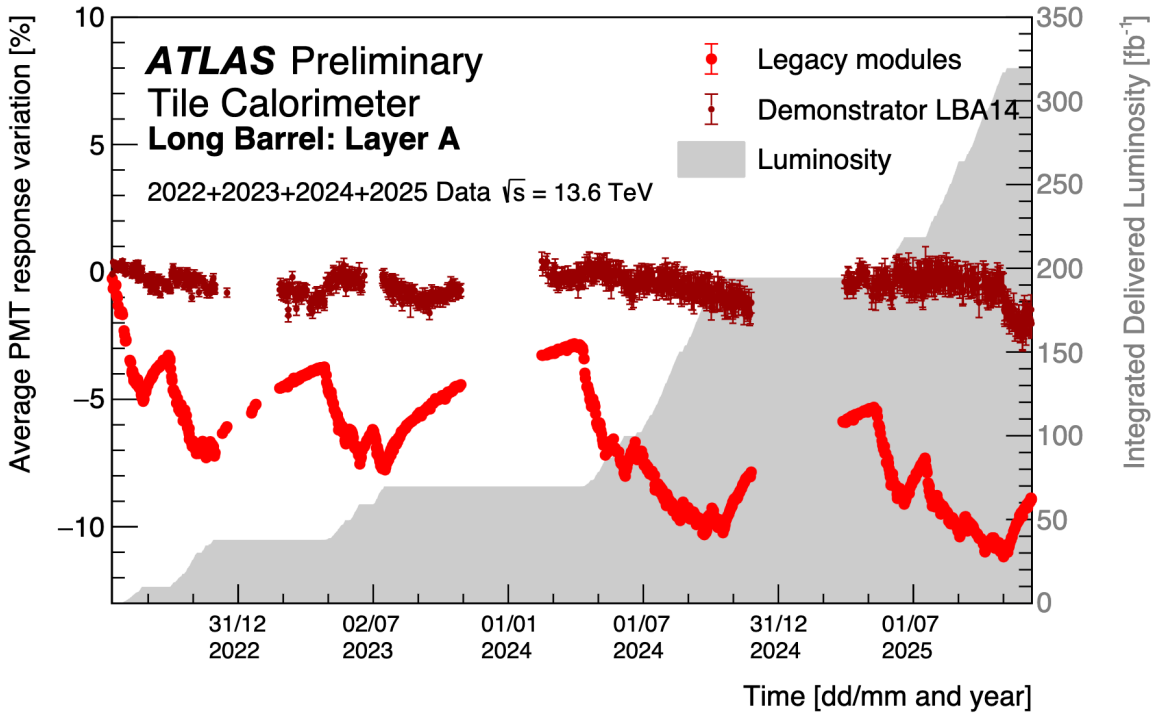


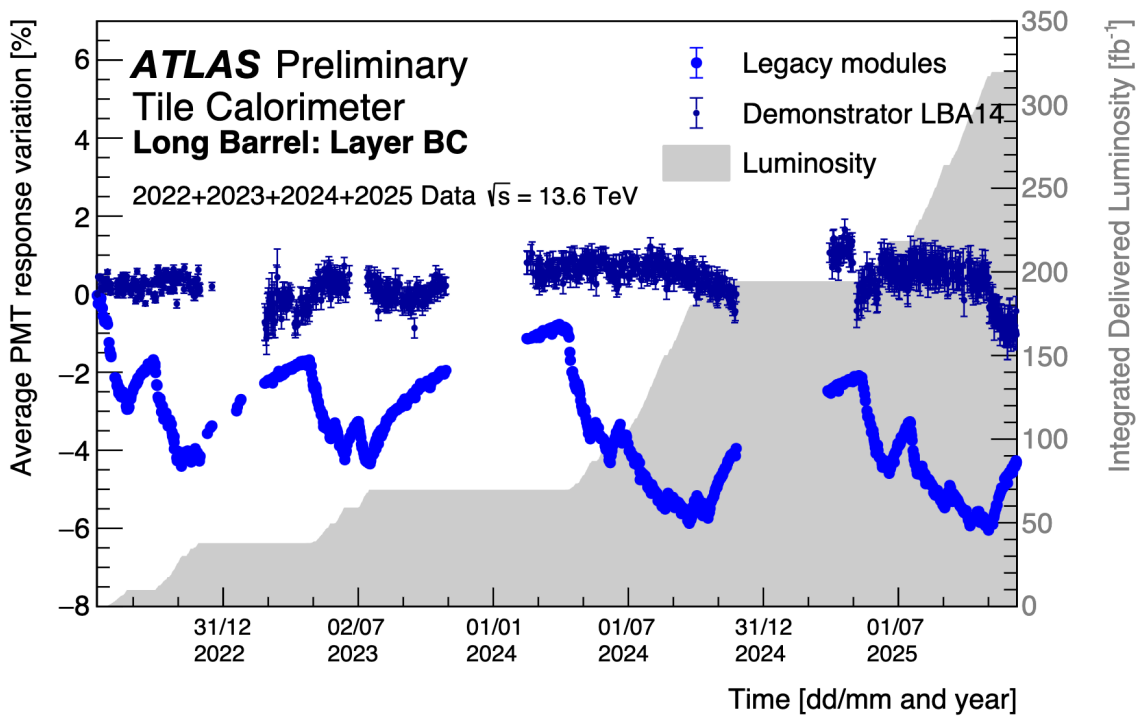




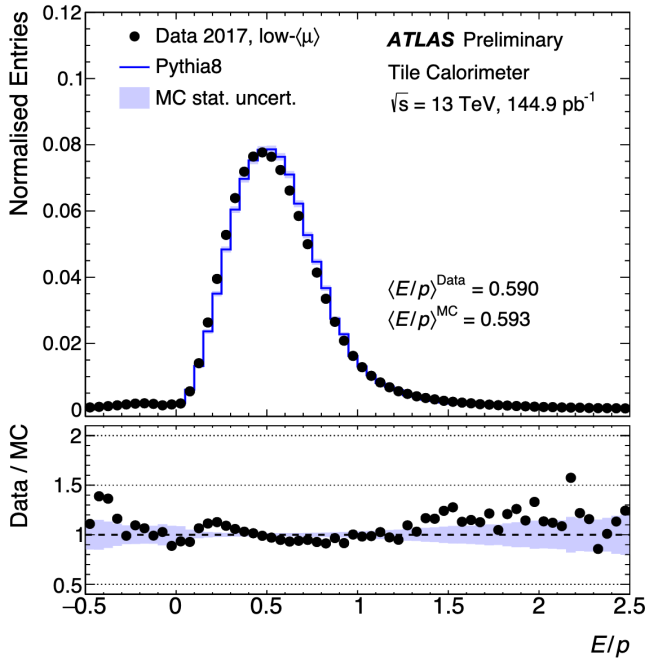


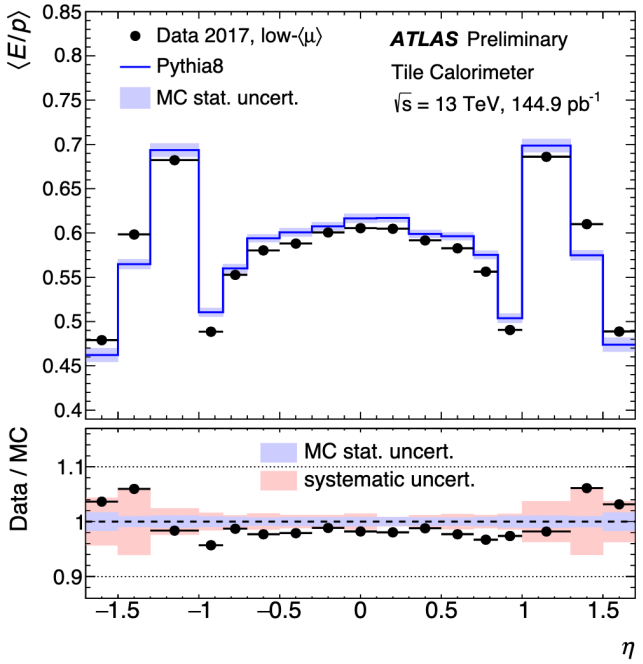
New PMTs

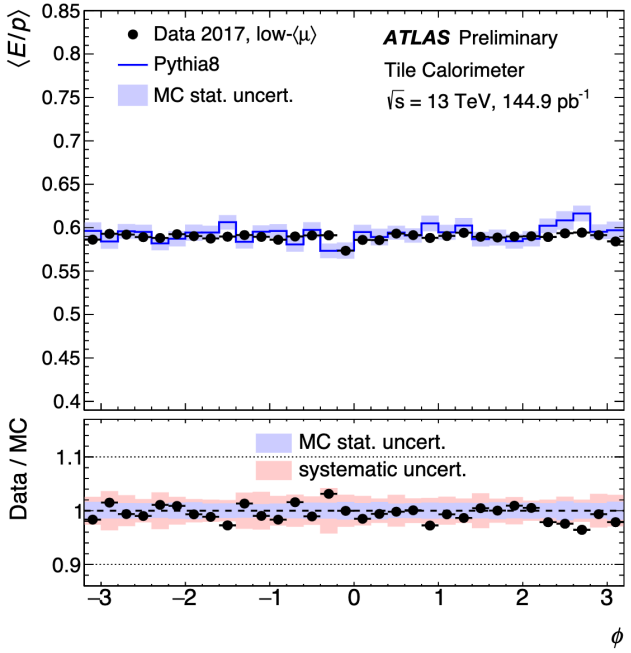

ATLAS Preliminary
Tile Calorimeter
Long Barrel: Layer A
2022+2023+2024+2025 Data √s = 13.6 TeV
Legacy modules
Demonstrator LBA14
Luminosity
Average PMT response variation [%]
Integrated Delivered Luminosity [fb⁻¹]
Time [dd/mm and year]
31/12 2022
02/07 2023
01/01 2024
01/07 2024
31/12 2024
01/07 2025

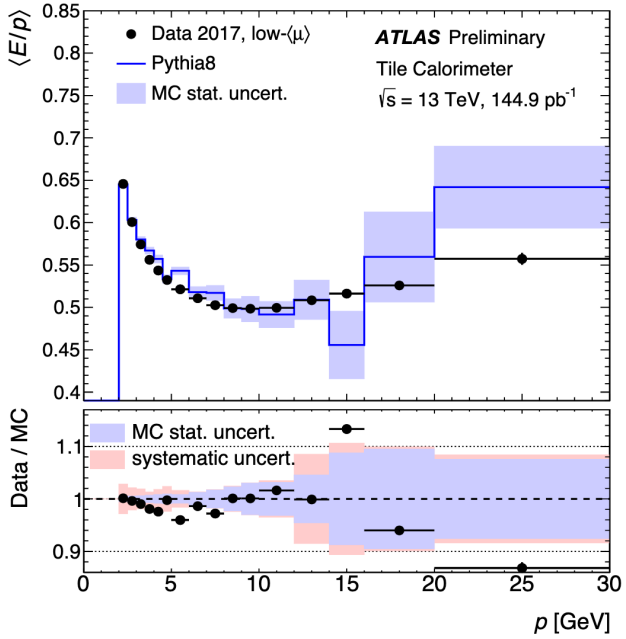

ATLAS Preliminary
Tile Calorimeter
Long Barrel: Layer BC
2022+2023+2024+2025 Data √s = 13.6 TeV
Legacy modules
Demonstrator LBA14
Luminosity
Average PMT response variation [%]
Integrated Delivered Luminosity [fb⁻¹]
Time [dd/mm and year]
31/12 2022
02/07 2023
01/01 2024
01/07 2024
31/12 2024
01/07 2025

Hadrons: simulation





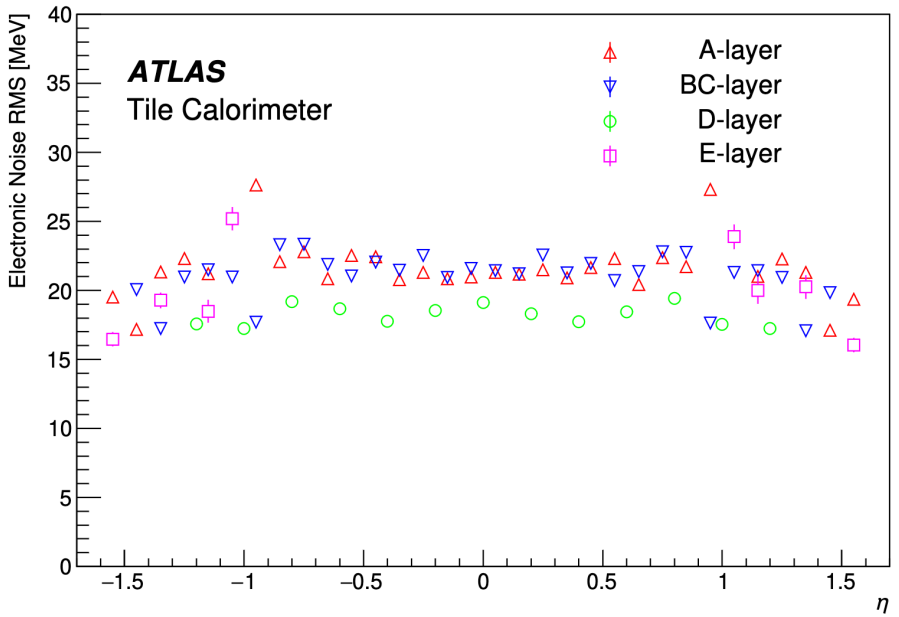




Noise description

- The TileCal noise description is a **fundamental input to calorimeter reconstruction** (topoclustering algorithms).
- Two main contributions: electronic noise, measured with pedestal data and independent of $\langle\mu\rangle$, and **pile-up noise** from in-time and out-of-time interactions.
- Pile-up noise is measured using **zero-bias data**: the RMS of the cell-energy distribution is measured versus $\langle\mu\rangle$, with the electronic noise fixed, to extract a pile-up noise constant for each cell layer.

Average electronic noise vs. η

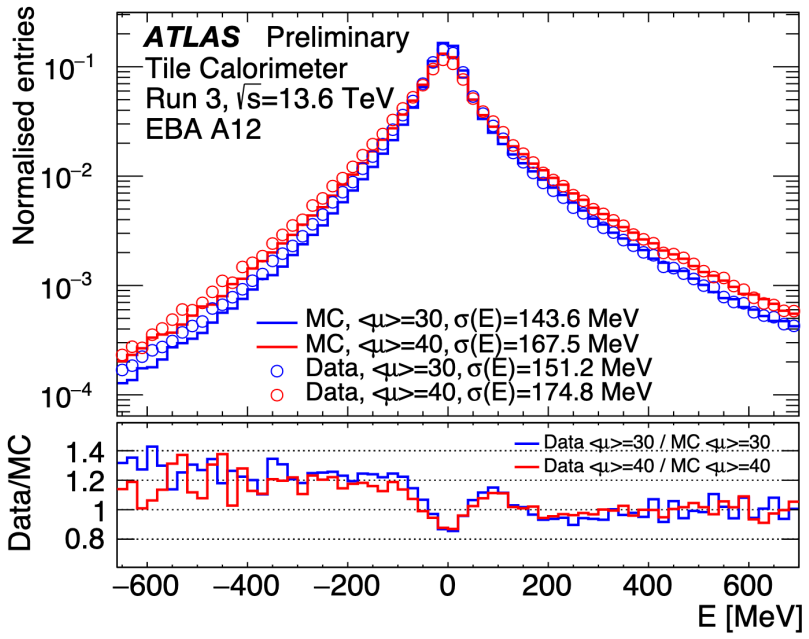


Eur.Phys.J.C 84 (2024) 12, 1313

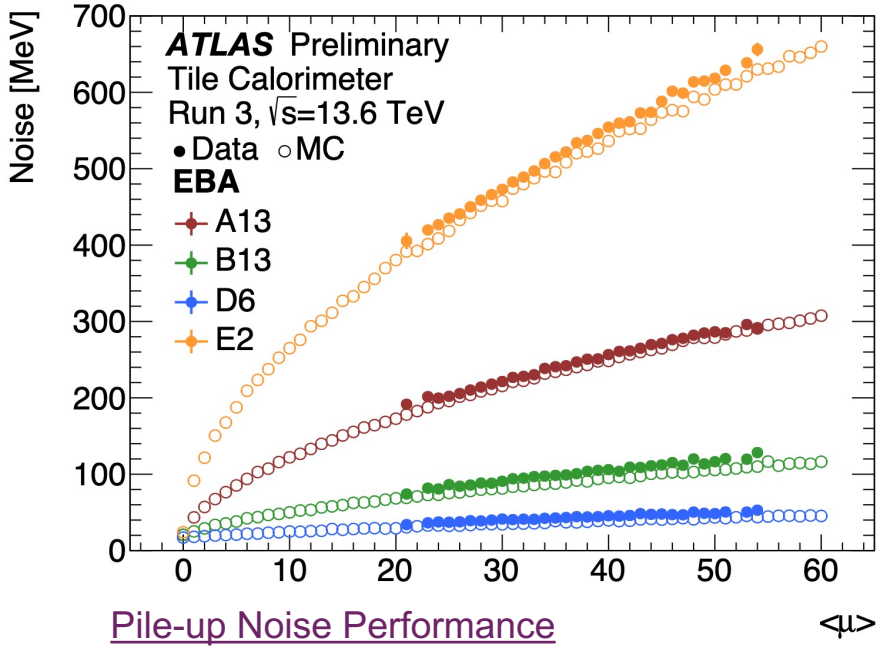
Noise description

- The TileCal noise description is a **fundamental input to calorimeter reconstruction** (topoclustering algorithms).
- Two main contributions: electronic noise, measured with pedestal data and independent of $\langle\mu\rangle$, and **pile-up noise** from in-time and out-of-time interactions.
- Pile-up noise is measured using **zero-bias data**: the RMS of the cell-energy distribution is measured versus $\langle\mu\rangle$, with the electronic noise fixed, to extract a pile-up noise constant for each cell layer.

Energy distribution in A12 for zero-bias data

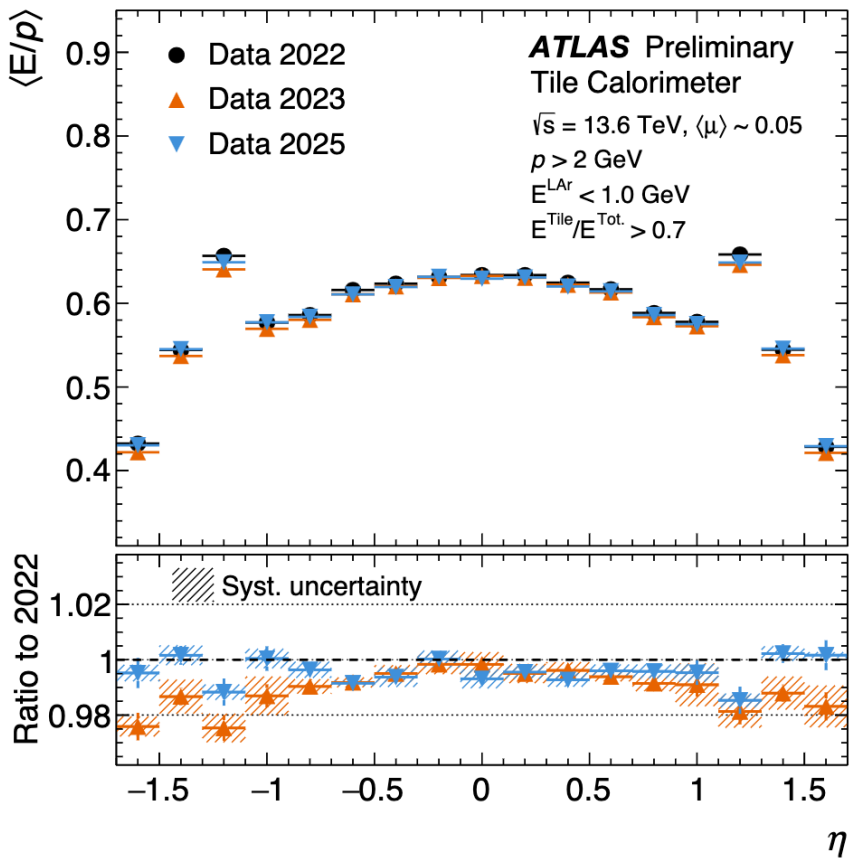


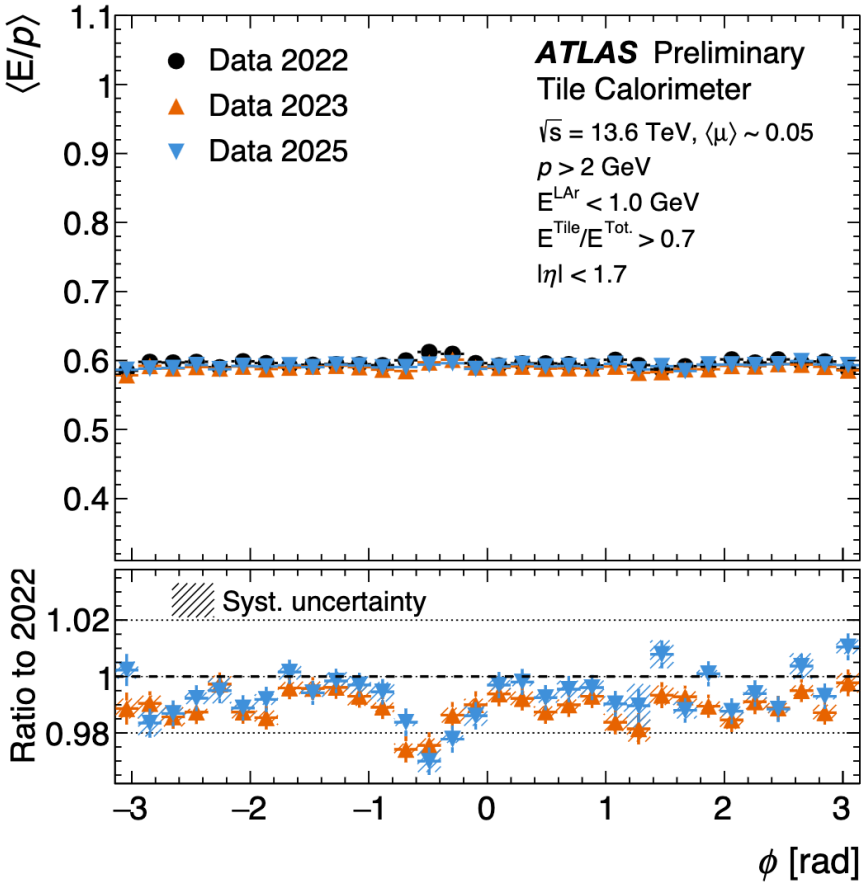
Total noise vs $\langle\mu\rangle$



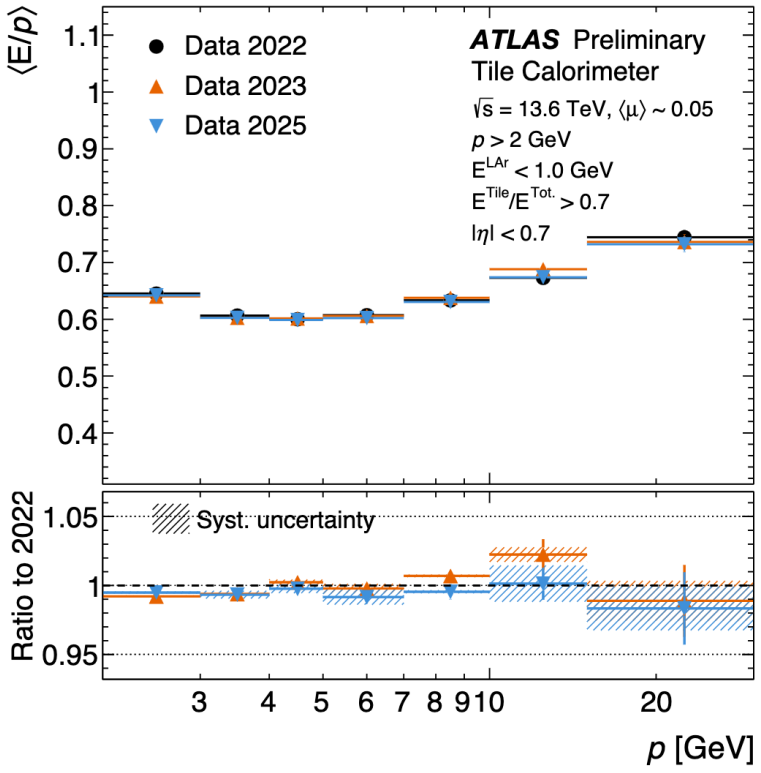
Pile-up Noise Performance public plots

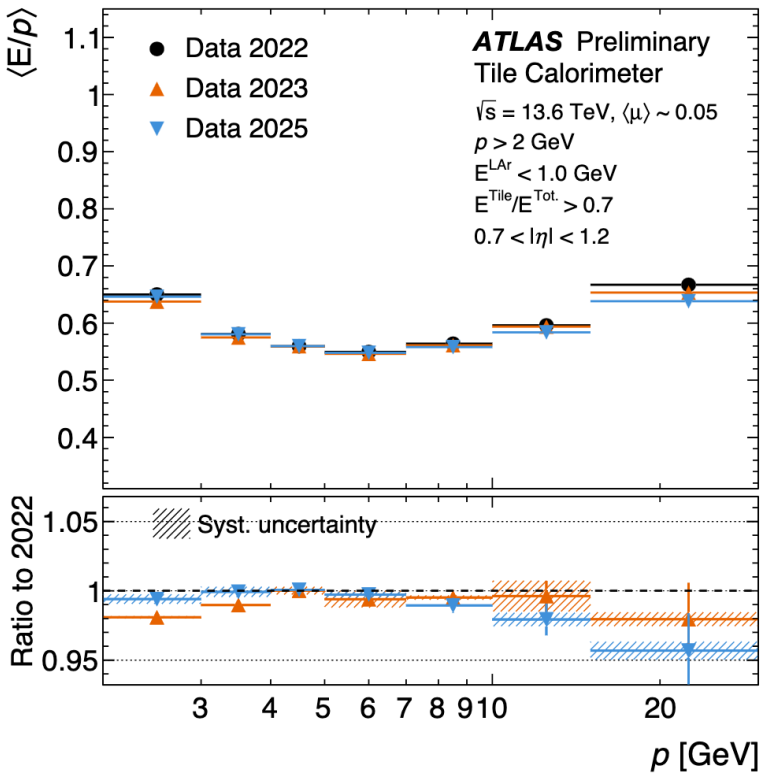
Hadrons: response stability

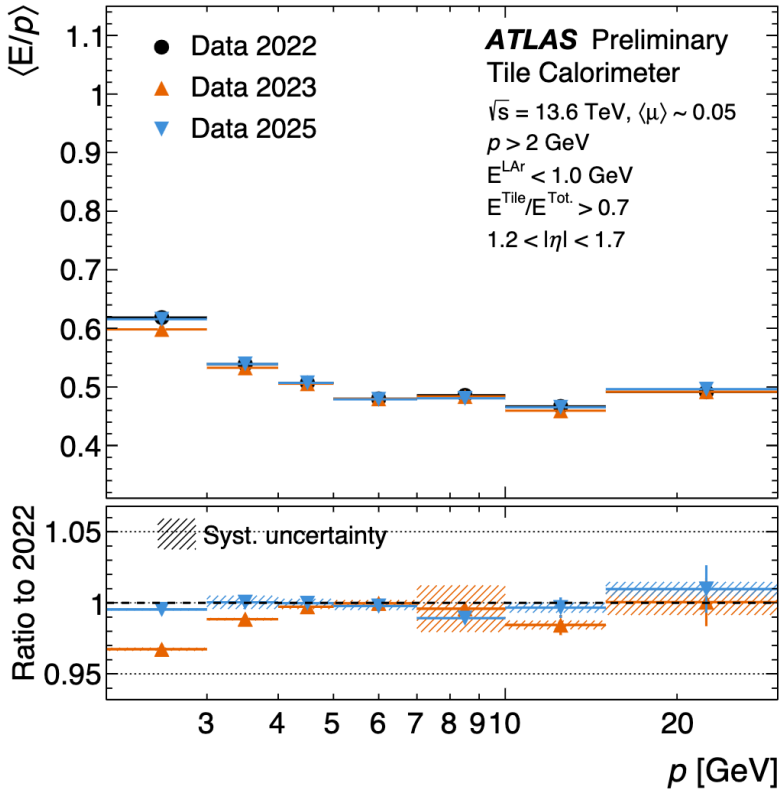




Hadrons: response stability

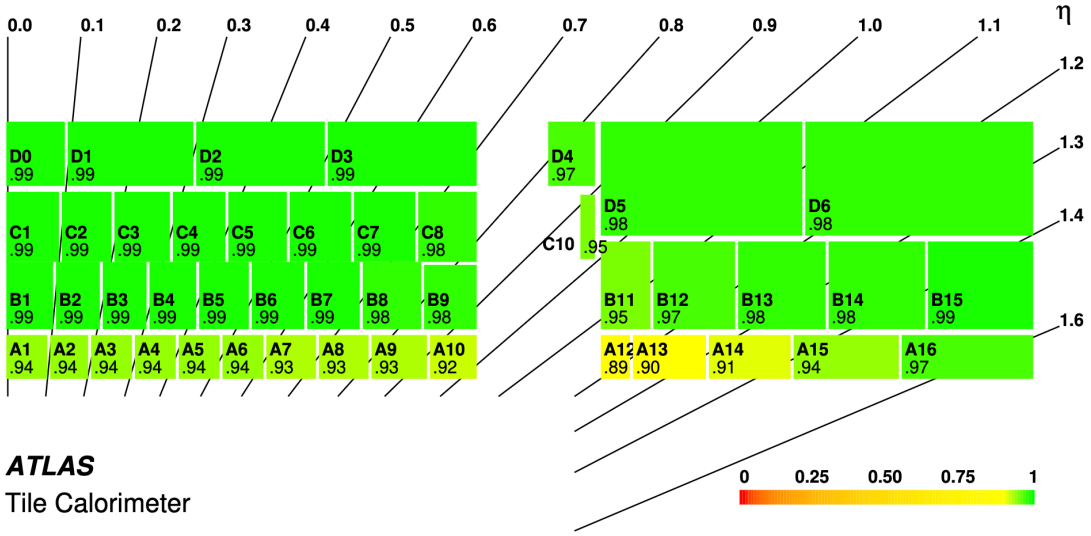




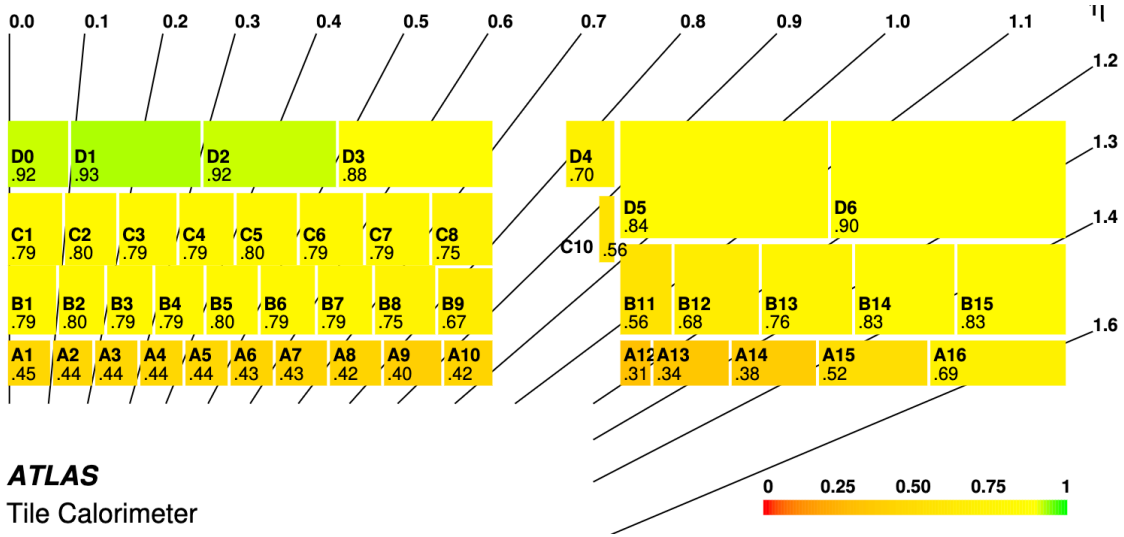


Long-term aging: response degradation extrapolations

Light yield degradation in Run 2



HL-LHC extrapolation of light yield degradation



Dose rate effects

$$I/I_0 = p_0 e^{-d/p_1}$$

